ADSORPTION CALORIMETRY IN SUPPORTED CATALYST CHARACTERIZATION: ADSORPTION STRUCTURE SENSITIVITY ON $Pt/\gamma\text{-}Al_2O_3$

A THESIS SUBMITTED TO
THE GRADUATE SCHOOL OF NATURAL AND APPLIED SCIENCES
OF
MIDDLE EAST TECHNICAL UNIVERSITY

BY

MURAT ÜNER

IN PARTIAL FULFILLMENT OF THE REQUIREMENTS
FOR
THE DEGREE OF MASTER OF SCIENCE
IN
CHEMICAL ENGINEERING

SEPTEMBER 2004

Approval of the Graduate School of Natural and Applied Sciences

Prof. Dr. Canan Özgen
Director

I certify that this thesis satisfies all the requirements as a thesis for the degree of Master of Science.

Prof. Dr. Timur Doğu
Head of Department

This is to certify that I have read this thesis and that in my opinion it is fully adequate, in scope and quality, as a thesis and for the degree of Master of Science.

Assoc. Prof. Dr. Deniz ÜNER
Supervisor

Examining Committee Members

Prof. Dr. İnci EROĞLU _____

Assoc. Prof. Dr. Deniz ÜNER _____

Prof. Dr. Ali ÇULFAZ _____

Asst. Prof. Dr. Erol ŞEKER _____

Asst. Prof. Dr. Halil KALIPÇILAR _____

I hereby declare that all information in this document has been obtained and presented in accordance with academic rules and ethical conduct. I also declare that, as required by these rules and conduct, I have fully cited and referenced all material and results that are not original to this work.

Name, Last name : Murat Üner

Signature :

ABSTRACT

ADSORPTION CALORIMETRY IN SUPPORTED CATALYST CHARACTERIZATION: ADSORPTION STRUCTURE SENSITIVITY ON $Pt/\gamma\text{-}Al_2O_3$

Üner, Murat

M.S., Department of Chemical Engineering

Supervisor: Assoc. Prof. Dr. Deniz ÜNER

September 2004, 69 pages

In this study, the structure sensitivity of hydrogen, oxygen and carbon monoxide adsorption was investigated by changing the metal particle size of Pt/Al_2O_3 catalysts. 2 % Pt/Al_2O_3 catalysts were prepared by incipient wetness method; the particle size of the catalysts was manipulated by calcining at different temperatures. The dispersion values for the catalysts calcined in air at 683K, 773K and 823K were measured as 0.62, 0.20 and 0.03 respectively. The differential heats of adsorption of hydrogen, carbon monoxide and oxygen were measured using a SETARAM C80 Tian-Calvet calorimeter. No structure dependency was observed for hydrogen, carbon monoxide or

oxygen initial heats of adsorption. The adsorbate:metal stoichiometries at saturation systematically decreased with increasing particle size. Hydrogen chemisorption sites with low and intermediate heats were lost when the particle size increased. On the other hand, oxygen and carbon monoxide initial heats and adsorption site energy distributions did not change appreciably with the metal particle size.

Keywords: Microcalorimeter, Adsorption Calorimetry, Structure Sensitivity, Catalysis, Supported Metals, Pt

ÖZ

DESTEKLİ METAL KATALİZÖRLERİNİN KARAKTERİZASYONUNDA ADSORBLANMA KALORİMETRESİNİN KULLANIMI: Pt/γ-Al_2O_3 KATALİZÖRÜ ÜZERİNDE ADSORBLANMANIN YAPISAL DUYARLILIĞI

Üner, Murat

Yüksek Lisans, Kimya Mühendisliği

Tez Yöneticisi: Doç. Dr. Deniz Üner

Eylül 2004, 69 sayfa

Bu çalışmada, Pt/Al_2O_3 katalizörü üzerinde hidrojen, oksijen ve karbon moksit gazlarının adsorblanmasının yapısal duyarlılığı incelenmiştir. Deneysel çalışma için ıslaklık başlangıcı metoduyla hazırlanan 2 % Pt/Al_2O_3 katalizörlerinin metal parça büyüklükleri farklı sıcaklıklarda kalsine ederek değiştirilmiştir. Hava ortamında 683 K, 773 K ve 823 K'de kalsine edilen katalizörlerin metal disperslenme oranları 0.62, 0.20 ve 0.03 olarak tespit edilmiştir. Hidrojen, oksijen ve karbon monoksit gazlarının adsorblanma ısısları SETARAM C80 Tian-Calvet kalorimetre kullanılarak tespit edilmiştir. Bu gazların temiz katalizör yüzeyindeki adsorplanma ısılarında yüzeyin yapısına duyarlılık gözlemlenmemiştir. Metal parçacık büyüklüğünün artmasıyla doygunluk noktasındaki adsorblanmış gaz:metal oranı düşmektedir. Hidrojenin adsorblandığı düşük ve orta enerji seviyelerindeki aktif siteler metal parçacık

büyüklüğünün artmasıyla yok olmuştur. Oksijen ve karbon monoksitte ise metal parçacık büyüklüğünün artmasıyla aktif sitelerin enerji dağılımında büyük değişiklikler olmamamıştır.

Anahtar Kelimeler: Mikrokalorimetre, Adsorblanma Kalorimetresi, Yapısal Duyarlılık, Katalizör, Destekli Metaller, Pt

To My Family,

ACKNOWLEDGEMENTS

I would like to thank my supervisor Assoc. Prof. Dr. Deniz ÜNER for her valuable support, encouragement and guidance, for her kind attitude throughout this study.

I would also like to thank all the members of CAC-TUS group.

The financial support for this project is provided by TÜBİTAK under research contract no MISAG 188.

TABLE OF CONTENTS

LIST OF TABLES

LIST OF FIGURES

NOMENCLATURE

ΔH_{ads}	Enthalpy change of adsorption
ΔG_{ads}	Gibbs-free energy change of adsorption
ΔS_{ads}	Entropy change of adsorption
θ	Fractional surface coverage
β	Heating rate
v	Frequency factor for the desorption
E_d	Desorption energy
E_{mc}	Activation energy for surface migration in the dissociatively chemisorbed state
E_{mp}	Activation energy for surface migration in the molecularly, physically adsorbed state
E_D	Bond dissociation energy
fp	Faction of portal sites occupied by ruthenium atoms
H	Hydrogen
k_B	Boltzmann constant
n_a	Number of moles of adsorbate
$N_{ads,x}$	Incremental amount of gas adsorbed upto dose x
M_{Pt}	Molecular weight of platinum
m_{cat}	Weight of catalyst
P	Pressure
Pt	Platinum
R	Gas constant

T	Temperature
q_{st}	Isosteric heat of adsorption
q_{int}	Integral heat of adsorption
q_{d}	Differential heat of adsorption
q_{c}	Heat of compression
U_{0}	Energy of adsorption
U_{g}	Molar internal energy of the gas
U_{a}	Molar internal energy of the adsorbate
V_{g}	Volume of gas-phase

CHAPTER 1

INTRODUCTION

When molecules from the gas phase strike the surface of the catalyst, they may be reflected back into the gas phase immediately, or remain on the surface long enough to build at the interface a concentration higher than in the gas phase. This phenomenon is referred as adsorption. The first step of a catalytic reaction at the surface of a solid catalyst is the adsorption of at least one reactant. This essential step can be studied independent of the catalytic reaction by the characterization of the adsorbed species formed on the catalyst in the presence of a single reactant (Dulaurent and Bianchi, 2000).

Adsorption can be considered in three states; physical adsorption, chemisorption and precursor states. Physical adsorption involves the forces of molecular interactions (dipole-dipole interactions), so often called as Van Der Waals adsorption. On the other hand, chemisorption involves the rearrangement of electrons of the interacting gas and solid, with consequential formation and rupture of chemical bonds. Physical adsorption is characterized by enthalpy changes that are small, typically in the range 10 to 40 kJ/mol, whereas heats of chemisorption are in the range of 80 kJ/mol to 400 kJ/mol (Thomas and Thomas, 1997). We shall also consider the

physisorption as a precursor state to chemisorption. Two types of precursor states can occur; intrinsic and extrinsic.

In the intrinsic precursor state the molecules strike empty surface sites, where they are trapped in a precursor state. The gas molecules are trapped in a transitory existence before being finally chemisorbed. In the extrinsic precursor state the molecules strike the filled sites and held there in a transitory state. Because of the mobility of the state, the rate of adsorption can be independent of coverage over a wide range of coverage. It is also possible that chemisorbed molecule to desorb back to a precursor state, where it has the chance to move to a different site, re-adsorbing and desorbing. Thus the chemisorbed state has the probability of becoming mobile through the precursor state (Doraiswamy, 1991).

In the adsorptionö the solid is called the adsorbent and the adsorbed substance the adsorbate. Adsorption is generally exothermic ($\Delta H_{ads} < 0$), as it occurs spontaneously ($\Delta G_{ads} < 0$) and leads to a more ordered state ($\Delta S_{ads} < 0$); According to the relationship:

$$\Delta G_{ads} = \Delta H_{ads} - T\Delta S_{ads} \qquad (1.1)$$

The heat evolved is called the heat of adsorption and can be measured experimentally. It is related to the energy of the bonds formed and thus represents a measure of the strength of the interaction (Solinas and Ferino, 1998).

Among several parameters which can be determined (i.e. amount and structure of the adsorbed species) the heat of adsorption appears as essential because it controls the coverage of each adsorbed species for given adsorption temperature and pressure (Dulaurent and Bianchi, 2000). There are several different types of heat of adsorption. Some of the definitions and the relations between them are;

Energy of adsorption (U_0): The potential energy difference between the lowest energy state of the molecule in the gas phase and its lowest energy state in the adsorbed phase. It represents the heat of adsorption at 0 K.

Isosteric heat of adsorption (q_{st}): The isothermal differential heat related to the differential heat of adsorption.

Integral heat of adsorption (q_{int}): Quantity of heat received by the system when n_a moles of gas are adsorbed at constant temperature at constant volume.

Differential heat of adsorption (q_d): The change of integral heat of adsorption with respect to change in the adsorbed moles.

The following relations exist between these quantities:

$$q_d = -(U_0 + \frac{3}{2} k_B T) \qquad (1.2)$$

$$q_{st} = q_d + k_B T = -(U_0 + \frac{1}{2} k_B T) \tag{1.3}$$

$$q_d = \left(\frac{\delta q_{int}}{\delta n_a} \right)_T \tag{1.4}$$

The detailed derivation of equation 1.3 is given in Appendix A from classical thermodynamics point of view.

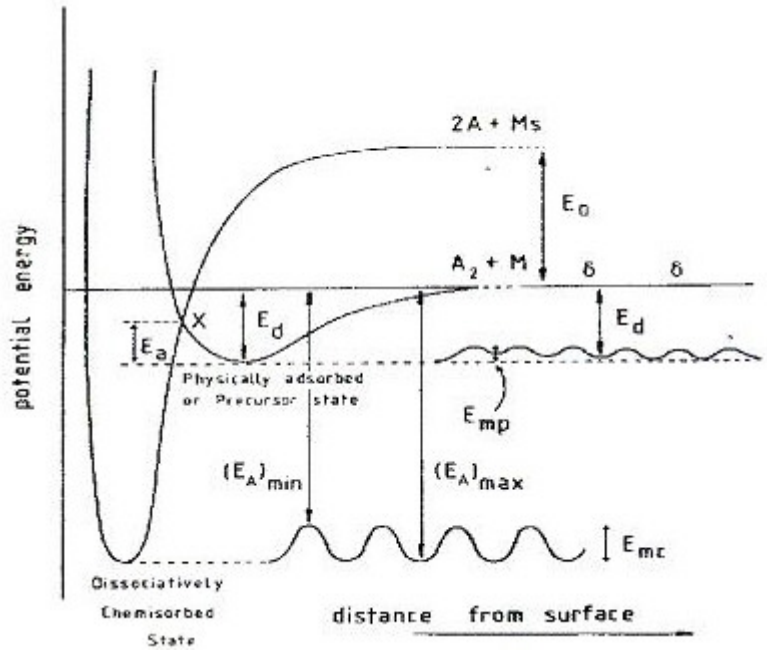

Figure 1.1: Potential-energy diagram for the approach of a diatomic molecule A_2 toward a surface M, E_{mc} and E_{mp} are the activation energies for surface migration in the dissociatively chemisorbed and molecularly, physically adsorbed states respectively. E_{mc} is the difference between the maximum and minimum energy of adsorption. E_D is the bond dissociation energy of desorption of A_2 (Thomas and Thomas, 1997).

The potential-energy diagram (Figure 1.1), of the kind introduced by Lennard-Jones, describes the energetics associated with the approach of a molecule to a solid surface. The first shallow potential energy minimum describes the physically adsorbed state. If, as the molecule proceeds nearer to the surface, chemical bonding can occur, then a deeper well is created. There is enough evidence for the importance of this physically adsorbed, or precursor, state in chemisorption. The most important being the fact that, for a wide range of gas-metal systems, chemisorption is a non-activated process. Whenever the crossover, X, of the physical adsorption and chemisorption curves lies below the potential-energy zero, dissociative chemisorption form the molecular state is non-activated (Thomas and Thomas, 1997).

There are essentially three methods for experimental determination of the heat of adsorption: (1) calculation from adsorption equilibrium data; (2) calculation from desorption kinetics data; (3) calorimetric measurement.

In regards to the first method, since adsorption processes are exothermic, we shall adopt the usual convention, assigning the differential molar adsorption heat, q, as the negative of the differential molar enthalpy change for the process. Isosteric adsorption heats, q_{st}, are determined under equilibrium conditions using the Clausius-Clapeyron equation:

$$q_{st} = -R\left(\frac{\partial \ln P}{\partial (1/T)}\right)_{\theta} \tag{1.5}$$

where R is the gas constant, P is the pressure, T is the temperature, and θ is the fractional surface coverage. Isosteres are usually obtained by

determining the pressure and temperature required giving a known coverage, and it is therefore important to monitor the coverage. To obtain the heat of adsorption, either isotherms or isobars are used, and once several have been obtained, a Clausius-Clapeyron plot is derived. However, the major disadvantage of this technique is that it can never be used to measure the heat of adsorption for an irreversible process.

The second method widely employed to estimate adsorption heats is through the measurement of the desorption energy, E_d. This method is more straightforward and is, hence, more commonly used. With a high pumping speed and a low heating rate, β, the desorption rate can be shown to be proportional to the observed pressure increase, P. The Redhead equation for first-order desorption is then used to relate E_d to the temperature at which a desorption peak occurs (D. A. King et al., 1998):

$$\frac{E_d}{RT} = \ln\left(\frac{vT}{\beta}\right) - 3{,}64 \qquad (1.6)$$

where v is the frequency factor for the desorption process. Formally, this only applies when E_d and v are independent of θ. Hence, the desorption energy can be determined at various initial coverages. This method is simple but has several disadvantages. It requires a precise knowledge of the desorption rate law, and this must also include information about how all of the kinetic parameters vary with coverage. Thus, there is a tremendous need for direct calorimetric measurements of adsorption energies. The most recent advances in calorimetry on surface was the development of the adsorption calorimetry, which provided the first opportunity to measure accurate, coverage-dependent adsorption heats on catalyst surface, where a direct

correlation with structural and spectroscopic results could be made (Brown et al., 1998; Yeo et al., 1997). The calorimetric determination of heat of adsorption does not require any model of the surface process and measure the heat directly. The method thus works both reversible and irreversible processes. Moreover, the calorimetric measurement occurs unlike the other two methods, at a fixed temperature.

1.1 Calorimetry:

Calorimetry is the direct measurement of heat and gives access to the energies of transformation and combination. Thermodynamic quantities that can be obtained by direct measurement are enthalpy, specific heat and heat capacity, which also give access to other values such as entropy and internal energy.

Among many uses of calorimetry purpose is the gas-solid interactions, which lead to a transformation of the sample (oxidation, reduction) and adsorption (physical, chemical). Moreover specific point considered is the heat of adsorption.

1.1.1 Principles of Calorimetry:

A calorimeter is basically consists of an experimental vessel placed in an external vessel. According to the quantities of heat exchanged between these two vessels, three main type of calorimeter can be identified.

1.1.1.1 Adiabatic Calorimeter:

In adiabatic calorimeters, the thermal insulation between the internal and external vessel is supposed to be perfect and the rise in temperature is measured within the internal vessel. The quantity of heat evolved or adsorbed can be calculated from this rise in temperature if the heat capacities of the calorimeter and of the reactants present are known.

1.1.1.2 Isothermal Calorimeter:

In isothermal calorimeters heat must not accumulate in the internal vessel, and the measurement made is often the thermal flux. An isothermal calorimeter is characterized by a vessel whose temperature must remain strictly constant. To achieve this, the evolved or adsorbed heat of the studied phenomenon must be compensated for as perfectly and as quickly as possible bringing in heat or pumping it out.

1.1.1.3 Tian-Calvet Calorimeter:

Tian-Calvet calorimeters (Figure 1.2), so called conduction or heat-flow calorimeters, represent an intermediate solution between the adiabatic and isothermal calorimeters. Thermocouples are used which simultaneously perform thermal conduction and measure the heat flow.

The principle of the Tian-Calvet calorimeter is that by increasing the thermal conductivity between the internal calorimetric vessel and its surroundings, it is possible to measure the thermal transfers by conduction directly (Figure 1.3). This increase in thermal conductivity is achieved by placing a

thermopile, which consists of thermocouples, between the internal and external vessel. The system becomes noticeably isothermal due to stabilization of the surrounding temperature by a precisely thermostated calorimetric block, which keeps the internal vessel at constant temperature.

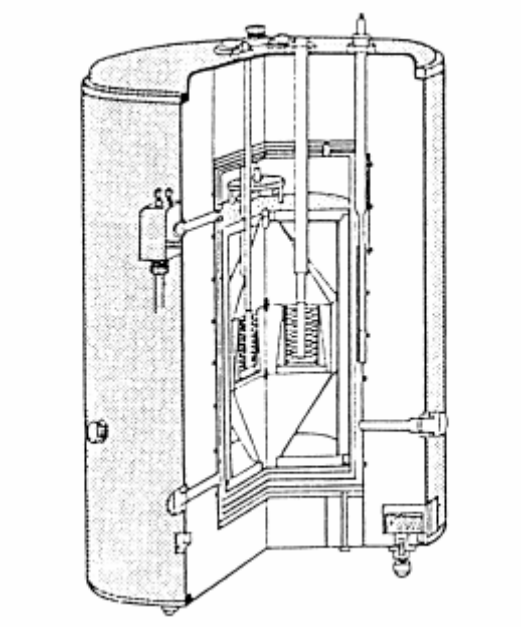

Figure 1.2: Tian-Calvet Microcalorimeter (Auroux, 1994).

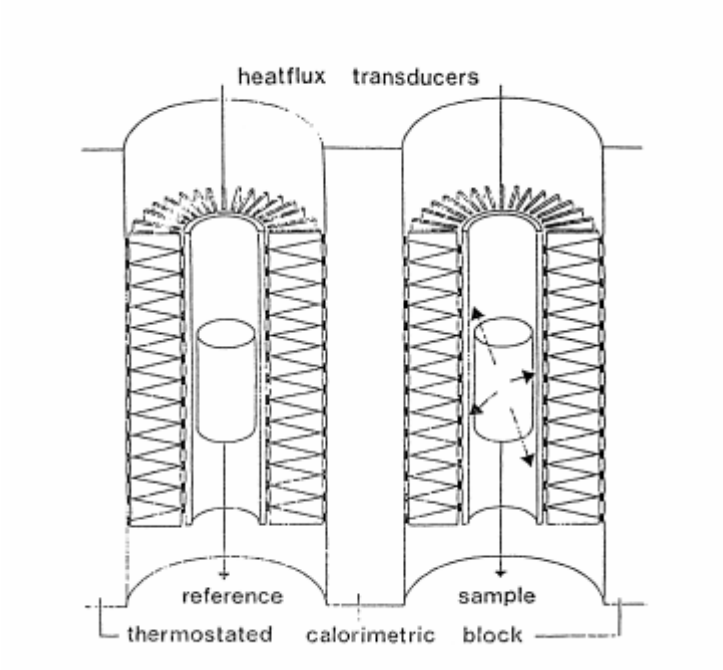

Figure 1.3: Microcalorimetic element (Auroux, 1994).

1.1.2 Use of Calorimeter:

There are many different types of applications of calorimeters and various possibilities of coupling with other methods of analysis. One of the distinguishing applications is the acid-base interaction. Adsorption of the basic molecules or acidic molecules on aluminas, zeolites and other oxides has been investigated by means of the calorimetry of the adsorption. Knowledge of the strength and number of acidic or basic sites in a catalyst is very important but measurement in the solid phase is very difficult. The strength of sites and their distribution are more precisely and more directly measured by the determination of the differential heats of adsorption of a basic or acidic probe molecule, depending on the solid.

In the study of surfaces with gas-solid interactions the following techniques are the ones used most often.

1.1.2.1 Coupling Calorimetry-Gas Chromatography:

The analysis of the gaseous phase of the sample can be done by chromatograph to see if there exists a decomposition, adsorption or desorption of gas. The reactor, either flow or pulse, containing the catalyst is placed in the calorimeter. By using pulse reactor the measurement of adsorption heats of a gaseous reactant on a solid or interaction heats between a gaseous reactant and preadsorbed species can be done. With a flow reactor it allows the kinetic study of catalytic reactions as well as the study of the activation or the aging of the catalyst.

1.2.2.2 Coupling Calorimetry-Volumetry:

A system that links microcalorimeter to the volumetric measurement of quantities of adsorbed reactants enables the study of gas-solid interactions and catalytic reactions. The volumetric determination of the adsorbed amounts of gas is performed in a constant-volume vessel in successive doses. The experiment consists of sending successive increments of the reactant gas onto catalyst and waiting for the thermal equilibrium after each increment. The aim is to minimize the volume of each increment in order to follow as closely as possible any changes as a function of the coverage. For every dose, the equilibrium data, such as the P_i, the adsorbed amount Δn_i, and the integral evolved heat Δq_{int}, are measured (Auroux, 1994).

CHAPTER 2

LITERATURE SURVEY

2.1 Adsorption of H_2, CO and O_2 on Pt Surfaces:

Many catalytic reactions are structure sensitive, the rate depends on the detailed geometrical structure of the surface atoms of the catalyst. Structure sensitivity usually manifests itself as a dependence of the rate per surface atom on the average size of the catalyst particles. The understanding is that the relative number of corner and edge sites increases dramatically with decreasing particle diameter, and these very low-coordinated surface atoms could have a substantially different ability to interact with the gas phase molecules. Norskov et al. (2002) have demonstrated that the heat of adsorption of a species is directly related to the local structure of the catalysts, the step sites are more active unless poisoned, and they bind the adsorbates more strongly. The amount of heat evolved during the adsorption process, called the heat of adsorption, is closely related to the adsorbate-substrate bond strength. Furthermore, the differential heat of adsorption can be dependent on the surface coverage of the adsorbate due to the lateral adsorbate-adsorbate interactions or due to the surface heterogeneity.

The structure sensitivity of CO oxidation reaction is observed for gas phase catalytic reactions (Zafiris and Gorte, 1993; Gracia et. al, 2003) as well as in anodic oxidation studies (Akemann et al., 1998). Both Zafiris and Gorte (1993) and Gracia et al. (2003) have measured lower activation energies for CO oxidation at lower dispersions. Zafiris and Gorte (1993) have attributed the structure sensitivity of CO oxidation to higher desorption rates over larger particles promoted by the repulsive interactions due to the higher CO coverages on larger planes. The oxidation of CO to form CO_2 reaction proceeds via the combination of a chemisorbed CO molecule with a chemisorbed oxygen atom, the latter produced through the dissociative adsorption of O_2 on the Pt surface. Due to the poisoning effect of the CO adsorption on the Pt surface, amount of and bond strength of adsorbed oxygen on the surface gains more importance. The limited amount of data on oxygen adsorption compiled in a previous publication (Uner et al., 2003) is quoted in Table 2.1 for reference. The adsorption heats strongly depend on whether the adsorption is molecular or dissociative. Once dissociated, oxygen forms strong bonds with the surface exceeding 250 kJ/mol. However, the adsorption of oxygen over metal surfaces is hampered by the low sticking coefficients on the surface. The dissociative sticking coefficient of oxygen was shown to increase exponentially with step concentration, adsorbed species at the steps are bound on the step edges, and dissociation almost exclusively takes place at the step sites (Wang et al., 1997 and references therein). The existence of the step sites was demonstrated to enhance the adsorption and dissociation of oxygen (Wang et al., 1997; Sljivancanin and Hammer, 2002).

Table 2.1 Adsorption modes, heats and coverages of oxygen adsorption over various surfaces of Pt

Surface	Adsorption mode	Saturation coverage (ML)	Sticking coefficient, S_0	$E_{a,\,des}$ (kJ/mol)	ΔH_{ads} (kJ/mol)	Reference
Pt(111)	dissociative		0.064		339±32	Yeo et al., 1997
Pt(110)	dissociative	0.35	0.34		332±10	Wartnaby et al., 1996
Pt(111)		0.25	0.06	213.4 -175.7		Campbell et al., 1981
Pt(S)-[9(111)x(111)]		0.5	0.06	205-171.5		Schwaha and Bechtod, 1977
Pt(111)	molecular	0.6			37±2	Gland et al., 1980
Pt(111)	dissociative	0.4			470±10	Gland et al., 1980
Pt(111)		0.25	0.048±0.006			Monroe and Merrill, 1980
Pt(111)		0.25				Puglia et al., 1995
Pt(111)	molecular peroxo				40.5	Nolan et al., 1999
Polycristalline Pt		0.75				Tong and Wan der Klink, 1995
Pt(111)	molecular		0.12			Cudok et al., 1994

NMR studies combined with heat of adsorption measurements indicated that hydrogen adsorption over mono and bi-metallic Ru/SiO_2 catalyst is structure sensitive: hydrogen chemisorption is more facile over low coordination edge and corner sites (Narayan and King, 1998; Savargonkar et al., 1998; VanderWiel et al., 1999; Kumar et al., 2000; Savargonkar et al., 2002). The structure sensitivity of hydrogen adsorption was reflected in the calorimetry data in terms of loss of sites with low and intermediate heats in the presence of Ag or Cu atoms. However, initial heats of adsorption were not influenced in the presence of Ag or Cu. The initial and integral heats of adsorption data presented in Table 2.2 for hydrogen over Pt do not change much with the particle size.

Table 2.2 Literature data of hydrogen adsorption over supported Pt surfaces

Catalyst	% Pt	Initial heat of adsorption (kJ/mol)	Integral heat of adsorption (kJ/mol)	Saturation coverage (μmol/g catalyst)	Dispersion (mol H ads/mol Pt)	Reference
Pt/SiO_2	1.2	93	66	38.6	1.18	Cortright and Dumesic, 1995
$Pt\text{-}K/SiO_2$	1.2	95	67	46.0	1.31	Cortright and Dumesic, 1995
$Pt\text{-}Sn/SiO_2$	0.93	92	59	16.1	0.51	Cortright and Dumesic, 1995
$Pt\text{-}Sn\text{-}K/SiO_2$	0.93	97	52	26.0	0.89	Cortright and Dumesic, 1995
Pt/SiO_2	4.0	91	67	69	0.51	Sharma et al., 1994
Pt/SiO_2	7.0	92	68	94	0.63	Sharma et al., 1994

Structure sensitivity of CO adsorption was theoretically investigated by Hammer et al. (1997). Their predictions on well-defined crystal planes

indicated strong structure sensitivity in the adsorption energy from one structure to the other. The existence of the step sites is being demonstrated to enhance the adsorption of CO (Karmazyn et al., 2003; Hammer et al., 1997; McEwen et al., 2003). Integral heats of CO adsorption on two different orientations of Pt single crystal surfaces are different beyond experimental errors (Table 2.3). But, the structure dependency of CO chemisorption is difficult to elucidate from the literature data collected over supported metal catalysts (Table 2.3).

Table 2.3 Literature data of CO adsorption over supported Pt surfaces

Catalyst	% Pt	Initial heat of adsorption (kJ/mol)	Integral heat of adsorption (kJ/mol)	Saturation coverage (μmol/g catalyst)	Dispersion (mol H ads/mol Pt)	Reference
Pt/SiO_2	1.2	144	104	48.7	1.18	Cortright and Dumesic, 1995
$Pt\text{-}K/SiO_2$	1.2	140	101	26.7	1.31	Cortright and Dumesic, 1995
$Pt\text{-}Sn/SiO_2$	0.93	135	83	19.6	0.51	Cortright and Dumesic, 1995
$Pt\text{-}Sn\text{-}K//SiO_2$	0.93	138	91	10.4	0.89	Cortright and Dumesic, 1995
Pt/SiO_2	4.0	140	105.1	130	0.51	Sharma et al., 1994
Pt/SiO_2	7.0	140	113.8	162	0.63	Sharma et al., 1994
Pt(221)	-	185	170	1.5 ML[1]	-	Karmazyn et al., 2003
Pt(111)	-	180±8	119.5	1 ML[1]	-	Yeo et al., 1997

Therefore, the objective of this study was to measure oxygen, hydrogen and CO adsorption heats to elucidate the energetic component of structure

[1] ML: Monolayer

sensitivity of adsorption over 2%Pt/Al_2O_3 by changing the particle size. Calcination temperature was selected as the parameter to manipulate the particle size in order to avoid complications that may arise due to the preparative chemistry.

2.2 Portal Model of Hydrogen Adsorption:

In general understanding, the supported metal catalysts consist of particles with sizes less than 10 nm. A significant fraction of surface atoms in such small crystallites occupy edge, corner, step, and kink sites. The fraction of these sites changes drastically with the size of the metal particle. Furthermore, because adsorption rates can be much greater at edge, corner, and defect sites than on planar surfaces, the rate of an adsorption process can depend on the density of these non-basal plane surface sites (Kumar et al., 2000)

Kumar et al., (2000) has studied the H_2 adsorption on Ru/SiO_2 and Ag-Ru/SiO_2 catalysts. By taking into account of the results of two previous studies: (1) addition of Ag to Ru/SiO_2 results in large decrease in the amount of hydrogen adsorbed (Savargaonkar et al., 1998) and (2)microcalorimetric measurements showing a the decrease of the hydrogen atoms that have intermediate and low heats of adsorption (Narayan, 1997), Kumar et al. (2000) has proposed that silver probably changes the kinetics of hydrogen adsorption by preferentially occupying low coordination sites of the metal particles. The Ruthenium edge and corner sites act as gateways or portals through which hydrogen dissociatively adsorbs onto vacant basal plane sites.

When the portals are blocked by Ag atoms, the result is a drastic decrease in the amount of hydrogen adsorbed.

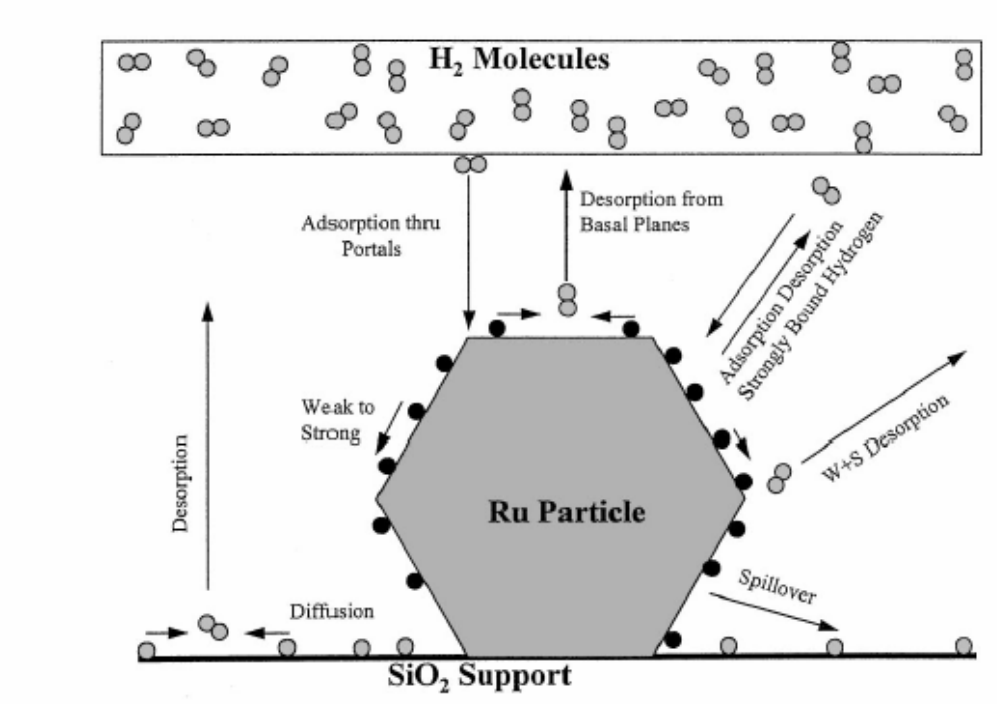

Figure 2.1: Schematic of portal model processes (Kumar et al., 2000).

The schematic view of the adsorption mechanism considered is given in Figure 2.1 and the key assumptions made for the steps of the adsorption mechanism can be summarized as;

(1) Hydrogen adsorption largely occurs through portal sites (edges and corners) at a rate independent of the hydrogen coverage on the metal.
(2) Dissociated hydrogen adsorbing through portal sites immediately moves to basal plane sites (i.e. portals cannot be occupied by hydrogen).

(3) Basal plane hydrogen binding site multiplicity is reduced to two types: strong binding and weak binding sites.
(4) No hydrogen is directly adsorbed from the gas phase onto weak binding sites; weak sites are populated only by hydrogen that first enters through portal sites.
(5) In contrast to weak binding sites, hydrogen can dissociatively adsorb directly from the gas onto adjacent strong binding adsorption sites without passing through portal sites.
(6) Weakly bound hydrogen can move to fill vacant strong binding sites.
(7) Two weakly or two strongly bound adjacent hydrogen atoms can desorb associatively.
(8) A weakly bound hydrogen atom can associatively desorb with strongly bound hydrogen.
(9) Weakly bound hydrogen atoms can spillover from metal particles to the support. The spillover process is assumed to be irreversible and first order in the coverage of weakly bound hydrogen.

The above assumptions lead to some dimensionless rate equations describing the hydrogen coverage on the metal particle, which produces results that are in good agreement with the experimental measurements (Figure 2.1).

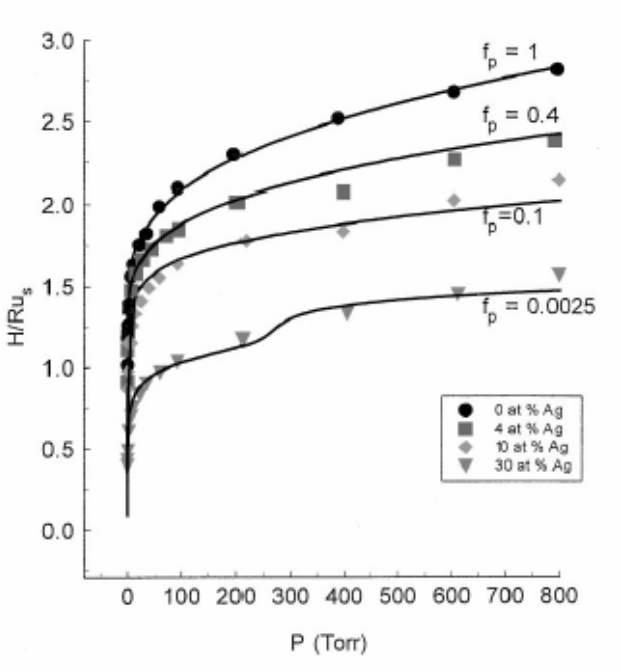

Figure 2.1: Hydrogen adsorption isotherms (symbols) and portal model predictions for various silver concentrations on Ru-Ag/SiO_2 at 400 K. The limiting cases of zero and 30 % silver were used to fit portal model parameters. Portal model predictions for the intermediate silver concentrations (4 and 10 at%) were calculated using fp as the only adjustable parameter (Kumar et al., 2000).

This portal model is able to explain the reduction in the amount of hydrogen adsorbed per surface ruthenium atom, upon addition of Ag to Ru/SiO_2 catalysts. Addition of Ag to Ru/SiO_2, selectively populating edge and corner sites results a decrease in the fraction of surface sites that act as portals. This model also provides a mathematical view for investigating the effect of structure sensitive adsorption processes on the overall kinetics of some catalytic reactions.

Smale et al (1989) have studied the effect of Cu addition to Ru/SiO_2 catalyst on the Ethane Hydrogenolysis. When Ru and Cu, immiscible in the bulk, are mixed, segregating element (Cu) preferentially populates the edge and corner sites of the supported crystallite (Ru). After these low coordination sites have been filled by Cu atoms, the formation of two-dimensional Cu islands on the basal planes of the particles began. The Monte Carlo simulation results for the occupation of the corner and the edge sites and the formation of the islands on the basal planes are given in the Figure 2.3.

The existence of the structure sensitivity has been studied in various ways. The effect of differently coordinated active metal atoms on the surface of the catalyst has been in the main concern. King and co-workers have studied various combinations on the Ru/SiO_2 catalyst with Ag and Cu for the reactions and the adsorption on the surface by changing the loading of the second metal. The main idea under these studies was that the selectively population of the second metal on the corner and the edge sites which have drastically different mission on both reaction and adsorption. Examining the catalyst in the range of pure active metal to the all corner and edge sites blocked by second metal yielded evidence for the structure sensitivity.

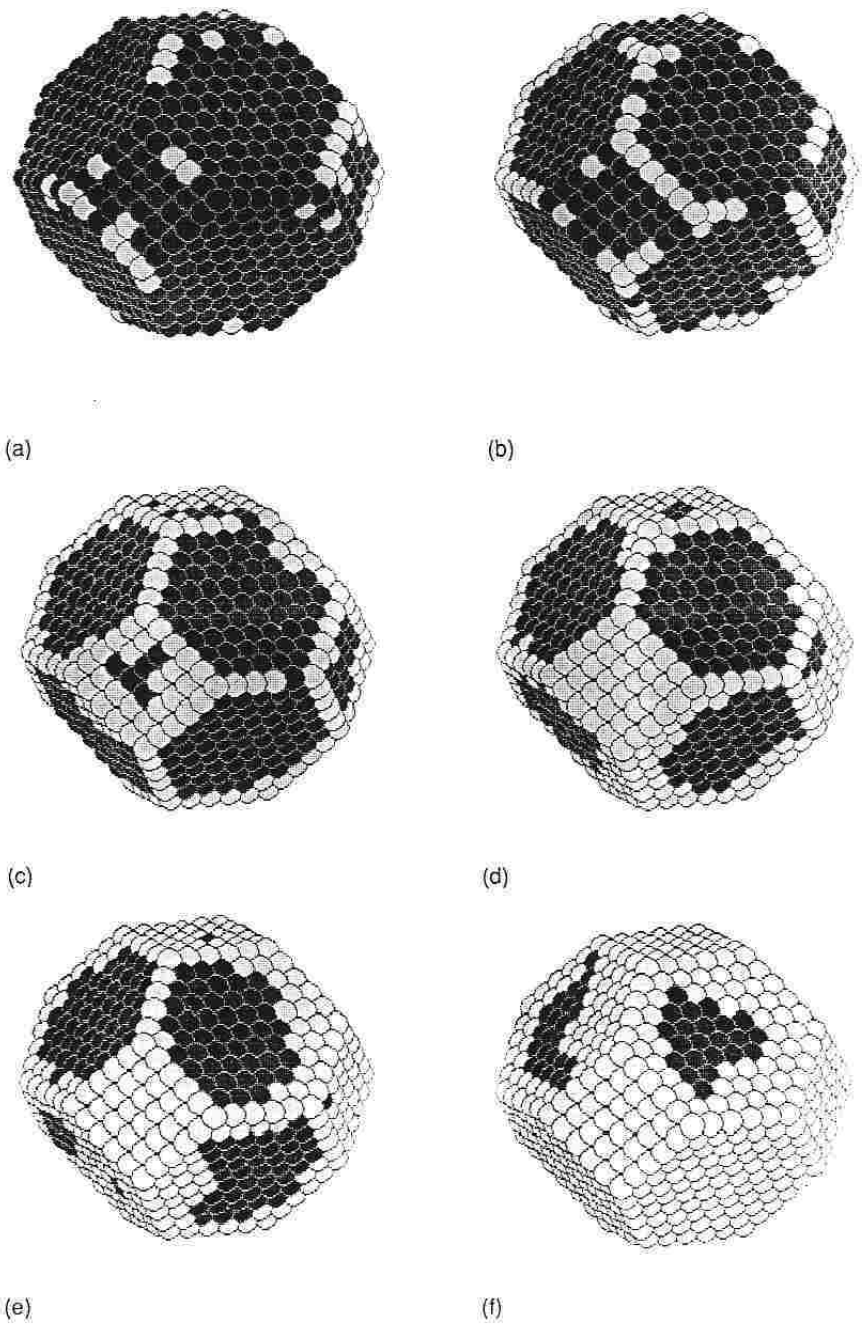

Figure 2.3: Monte Carlo simulation results for Ru-Cu/SiO_2 catalysts with a total metal dispersion of 30%; (a) 2% Cu, (b) 5% Cu, (c) 10% Cu, (d) 15% Cu, (e) 20% Cu, (f) 30% Cu (Smale et al., 1989).

Given that corner and edge sites have substantially different ability for the adsorption of the molecules on the surface, changing the relative amounts of these sites by any means would also yield similar results.

The amount of the corner and the edge sites present in the Pt changing with the particle size was simulated by means of Monte Carlo simulation (Sthrol and King; Schimpf et al., 2002). Dispersion was used as the representative and easily measurable factor of the metal particle size. From Figure 2.4, it can be easily concluded that by increasing the dispersion of the catalyst, the amount of the corner and the edge sites can be increased.

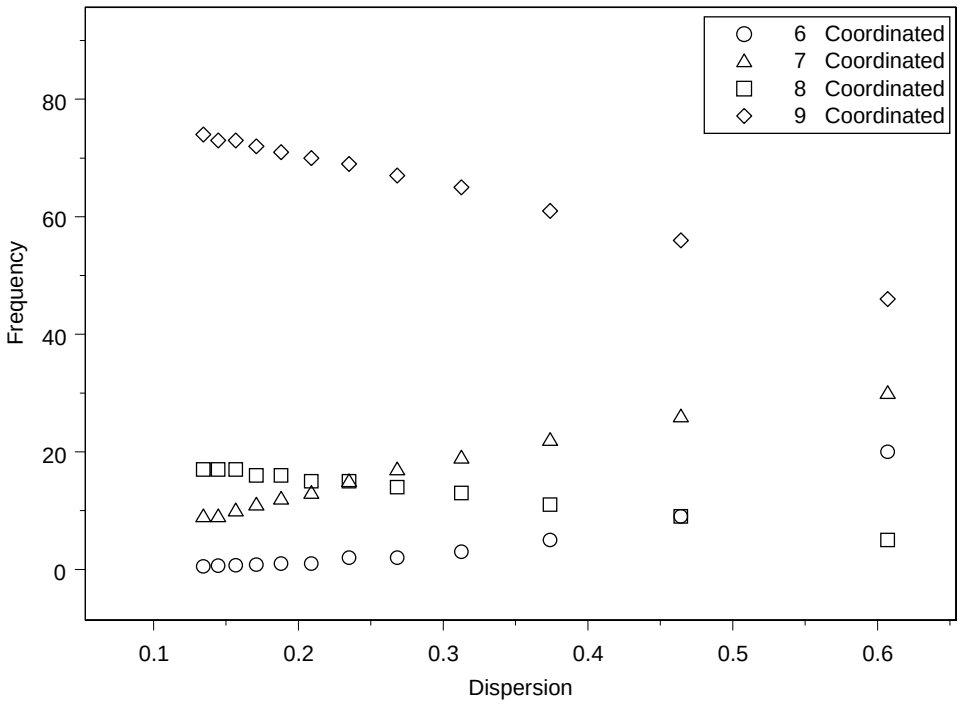

Figure 2.4: Monte Carlo simulation results; surface concentration of different sites with respect to dispersion for Pt (Sthrol and King).

CHAPTER 3

EXPERIMENTAL

The experimental study mainly based on microcalorimetry measurements. For catalyst characterization adsorption experiments were performed.

3.1. Sample preparation:

All of the samples were prepared by incipient wetness impregnation of Pt from a solution of tetraammine platinum (II) chloride hydride (Johnson Matthey) on dried γ-Al_2O_3 (Johnson Matthey, 65 m^2/g BET surface area). Before catalyst preparation the amount of distilled water needed to bring the γ-Al_2O_3 to the incipient wetness was determined. Approximately 2 ml of solution per gram of support was needed to bring about incipient wetness. The impregnation solution was prepared by dissolving an appropriate amount of $PtCl_2(NH_3)_4.H_2O$ salt in distilled water. The slurries obtained after impregnation were dried overnight at room temperature and at 400 K for two hours. The catalyst prepared as such was divided into three portions and each portion was calcined in air at a different temperature for four hours. The calcination temperatures were selected as 410, 500 and 600 ^oC.

3.2. Adsorption Measurements:

Adsorption measurements were conducted on a home built adsorption apparatus based on design of Tapan (1999): a multi-port high-vacuum Pyrex glass manifold with a volume of 162 cm^3 in connection with a turbo molecular pump (Varian Turbo V70D) backed by a mechanical pump (Varian SD-40) (Figure 3.1).

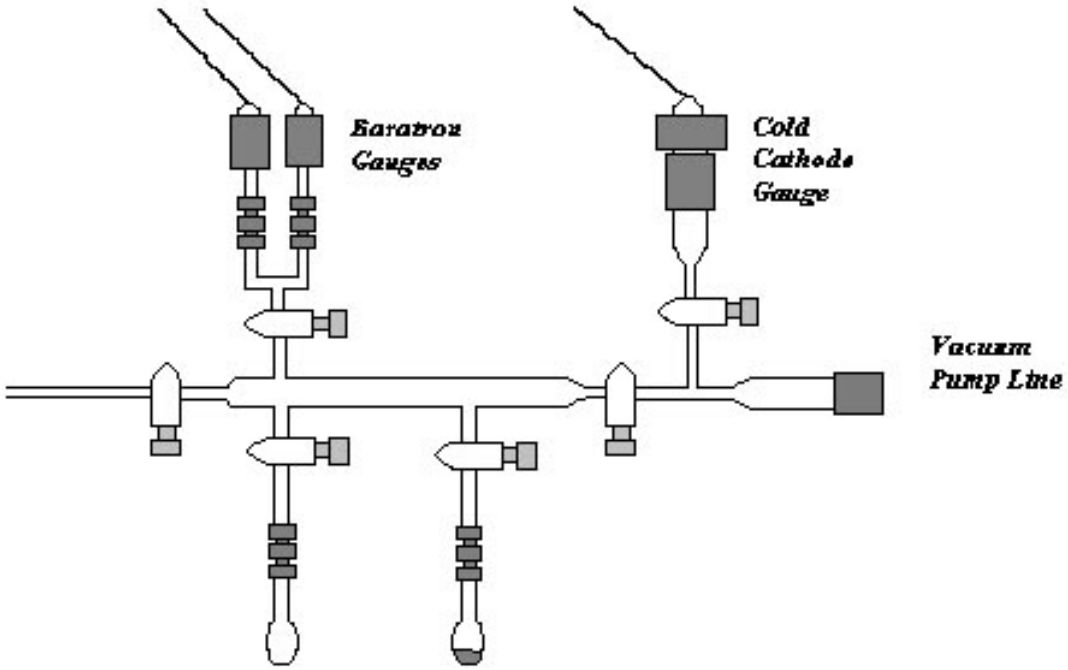

Figure 3.1: Home built multi-port high-vacuum Pyrex glass manifold.

In order to minimize hydrocarbon impurities in the manifold, high-vacuum greaseless, bakeable stopcocks with Teflon plugs and FETFE O-ring seals (Ace Glass) were employed to manipulate gas storage and/or dosage. The

manifold was capable of a vacuum better than 10^{-6} Torr after bake-out. A cold cathode gauge (Varian 524-2) monitored pressures below 10^{-3} Torr. Pressures from 10^{-4} to 10^{3} Torr were measured by two capacitance absolute pressure gauges (Varian CeramiCel). Catalyst samples were held in a Pyrex cell, a small heating mantle connected to a Variac was used to adjust the temperature in the cell.

All catalyst samples were treated inside the Pyrex cell. 1 g of sample was loaded into the cell, which was then attached to one of the sample ports of the manifold. The catalysts were reduced *in-situ* according to the following recepie: Approximately 100 Torr of helium was dosed in the manifold, the temperature of the heating mantle surrounding the cell was raised to 423 K for about 30 min to remove the residual water on the sample. The sample was then evacuated, 100 Torr of H_2 was dosed on the sample and the temperature was gradually raised to 623 K. At this temperature the sample was evacuated, fresh hydrogen at 750 Torr was dosed for 30 min. Hydrogen was replenished every 30 min. until the catalyst was exposed to hydrogen atmosphere at 623 K for at least 2 hours. After the reduction the catalyst was evacuated for 1 hour and cooled down to room temperature during final evacuation. The dispersion measurements were performed according to the method described by Uner et al. (1995) (see App. B for deatails of the experimental procedure). After collecting the total and weak hydrogen adsorption isotherms, the zero pressure values were obtained by extrapolating the data, the difference between the total and weak isotherm zero pressure values were reported as the strong hydrogen amounts. This value was used as the metal dispersions by assuming 1H : 1Pt stoichiometry for the strongly bound hydrogen. For sample calculations see Appendix B.

3. 3. Microcalorimetry:

Heat of adsorption measurements were conducted on Setaram C-80 Tian-Calvet Calorimeter coupled to the multi-port high-vacuum Pyrex glass manifold, similar in design to the manifold described in section 3.2. In this manifold a Pfeifer turbo molecular pump station backed by a diaphragm pump was used (Figure 3.2). The pressure measurements were done by a Baratron gauge (Varian CeramiCel) in the range of 10^{-4}-10 Torr. The details of the home made Pyrex sample and the reference cells for the calorimeter and the schematics of the set up are given in Uner et al. (2003).

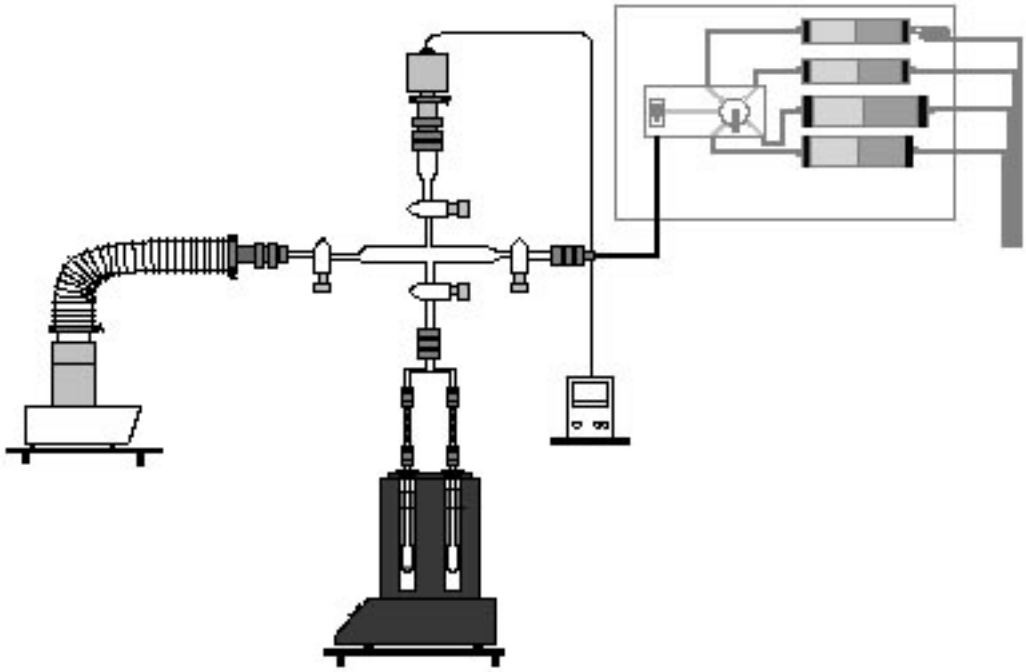

Figure 3.2: Setaram C-80 Tian-Calvet Calorimeter coupled to the multi-port high-vacuum Pyrex glass manifold.

The sample and the reference cells were connected to each other and to the vacuum manifold by a Pyrex Tee. Stainless steel bellows were used to connect the sample and the reference cells to the tee. All of the connections were made of stainless steel Cajon Ultra Torr unions. Thermal insulation of the home made cells were followed from the original design of the sample cells of Setaram: in order to avoid convective currents surrounding the sample cells, three aluminum rings were placed around the sample tube. The aluminum rings were supported by concentric glass tubes placed outside the sample tube.

0,3 gr of pre-calcined and pre-reduced sample was loaded into the sample cell, which was then attached to one end of the tee connection and inserted into the sample port of the microcalorimeter. The other end of the tee connection was attached to an empty sample cell inserted into the reference port of the microcalorimeter. The reduction procedure described above was followed except the high pressure H_2 dosing temperature reduced to 543 K due to the maximum allowable temperature limit of the microcalorimeter. After the reduction process the catalyst was cooled down to 303 K during final evacuation. The cooling from 543 K to 303 K and establishing the base line in Setaram C-80 Tian-Calvet Calorimeter takes nearly 12 h. so the cooling procedure was conducted overnight. After establishing the base line at 303 K, the differential heats of adsorption were measured by introducing small amounts of gas into the sorption chamber. The amount adsorbed and heat evolution data were recorded up to the point where there was no heat signal detected upon incremental gas dosing to the limit of the pressure measurement (10 Torr).

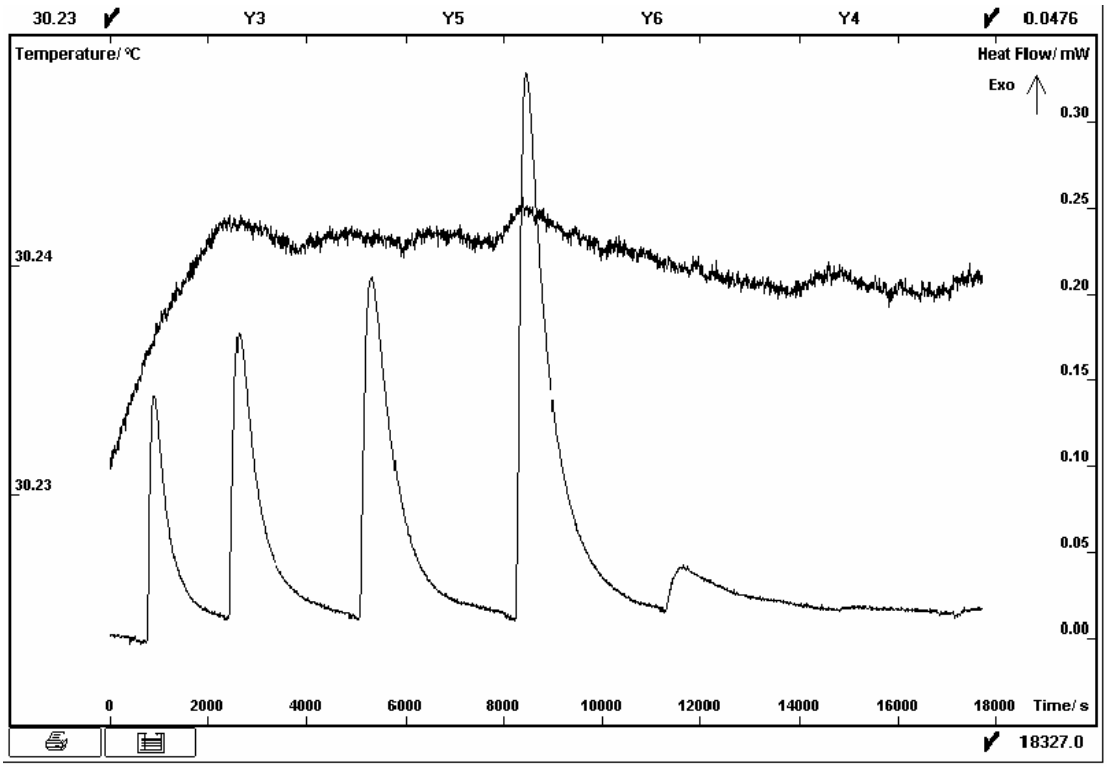

Figure 3.3: Typical adsorption experiment output of Seteram C-80 Microcalorimeter.

The heat evolved during the introduction of successive doses of gas was obtained from the area under the heat flow peaks (Figure 3.3). Having calculated the adsorbed amount of the gas at each dose from the pressure measurements by assuming the ideal gas law, from eqation 1.4 the differential heat of adsorption at each instant was calculated. In order to obtain the differential heat of adsorption of a gas until saturation over one catalyst sample, two days of experimentation is required.

CHAPTER 4

RESULTS AND DISCUSSION

4.1 Volumetric Chemisorption:

The volumetric chemisorption experiments performed for all the catalysts calcined at different temperatures to obtain the dispersion values, i.e., the ratio of the metal atoms exposed to total metal atoms available. The result of the adsorption experiment for the catalyst calcined at 410°C is given in Figure 4.1. (The results of the adsorption experiments are given in Appendix B)

The hydrogen adsorption amounts are presented in Table 4.1 as a function of calcination temperature. It can be seen from the data presented in Table 4.1 that the catalyst particle sizes could be manipulated by changing the calcination temperature as measured by the strongly adsorbed hydrogen stiochiometries. On the same table the saturation coverages of all adsorbates as measured by calorimetry are also presented for comparison.

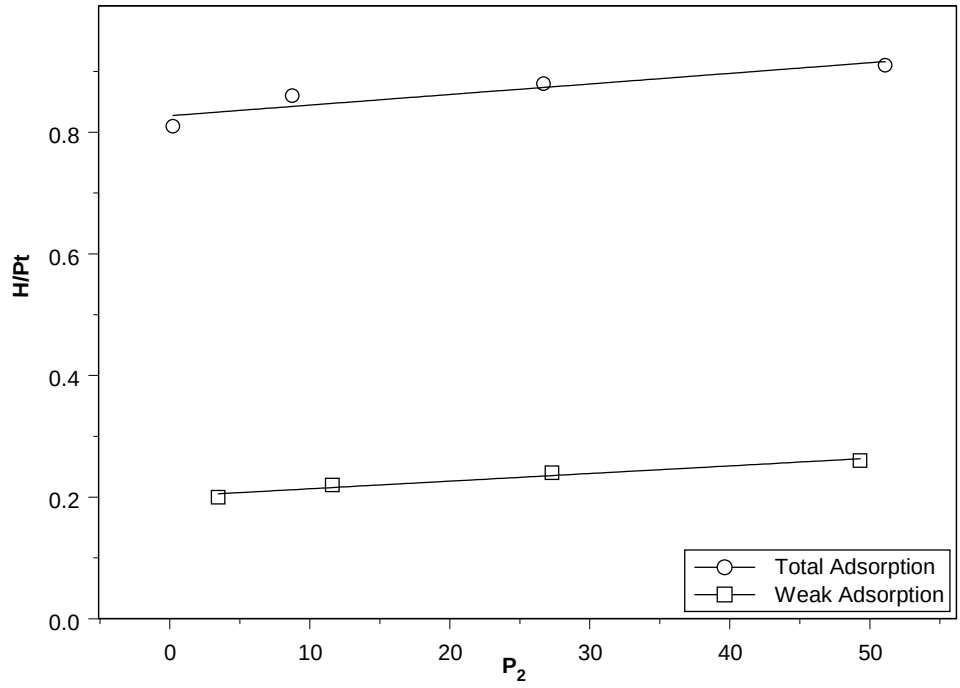

Figure 4.1: Change of the Hydrogen atoms bonded to Pt atoms with H_2 gas pressure.

Table 4.1 Total, weak and strong hydrogen to platinum stoichiometries calculated form the measured pressure data by volumetric chemisorption compared with the saturation coverages measured by microcalorimetry over 2%Pt/γ-Al_2O_3 calcined at different temperatures

	By calorimetry			By volumetric chemisorption		
Calcination temperature (^oC)	CO saturation coverages (CO/Pt_{total})	O saturation coverages (O/ Pt_{total})	H saturation coverages (H/Pt_{total})	Total hydrogen amounts (H/Pt_{total})	Weak hydrogen amounts (H/Pt_{weak})	Strong hydrogen amounts (H/Pt_{strong})
410	0.20	0.15	>0.7	0.83	0.20	0.63
500	0.10	0.12	0.20	0.26	0.06	0.20
600	0.04	0.06	0.08	0.09	0.05	0.04

4.2 Heat of Adsorption:

Hydrogen heat of adsorption data was plotted against hydrogen coverage Figure 4.2. The coverages were determined as the ratio of the hydrogen adsorption amounts at each instant to the total hydrogen amounts measured from chemisorption experiments. The heat of adsorption data was evaluated as per mol of atomic hydrogen adsorbed. The structure sensitivity of hydrogen adsorption is evident from the data presented in Figure 4.2.

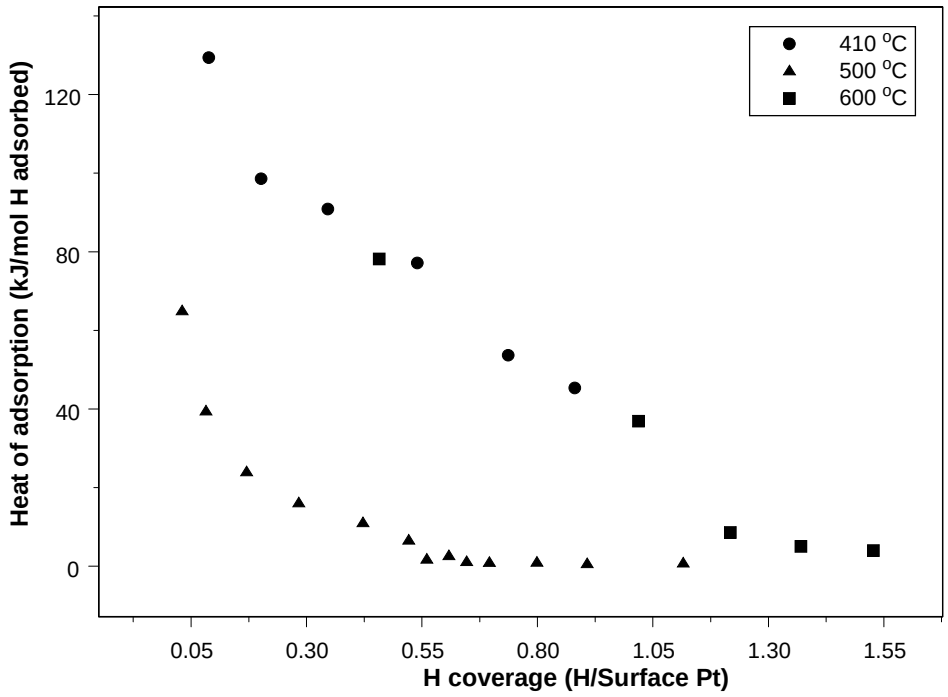

Figure 4.2: Differential heat of hydrogen adsorption over 2% Pt/γ-Al_2O_3. The temperatures indicate the calcination temperature of the catalysts.

As observed by Narayan and King (1998) and Savargoankar et al. (1998) over bimetallic catalysts, our catalysts have lost hydrogen adsorption sites with low and intermediate energies as the particle size increased, for the catalyst calcined at 500 ^{o}C. On the other hand, the heat of adsorption data of hydrogen over the catalyst calcined at 600 ^{o}C fall on the same curve as the data of the catalyst calcined at 410 ^{o}C. For the catalyst calcined at 600 ^{o}C, due to the low number of surface sites available for chemisorption, the sites with high initial heats could not be sampled. Narayan and King (1998) and Savargoankar et al. (1998) have attributed the sites with low and intermediate heats to planar surfaces over the catalyst particles. Our expectations of a catalyst calcined at 600 ^{o}C is to have mostly planar surfaces and the heats of adsorption of hydrogen values measured over these surfaces indicate that planar surfaces dominate over the catalyst calcined at 600 ^{o}C.

Oxygen adsorption data was also plotted in terms of dissociated oxygen coverages and heats per mol of atomic oxygen (Figure 4.3). The coverages were based on the saturation coverage over the catalyst as measured by calorimetry. It is important to note here that the differential heat of adsorption curve of oxygen over the catalyst calcined at 600 ^{o}C lies systematically above the differential heat of adsorption curve of the other catalysts. This can be interpreted as a particle size effect, over larger particles Uner et al. (2003) has measured higher heats over Pt/TiO_2 particles.

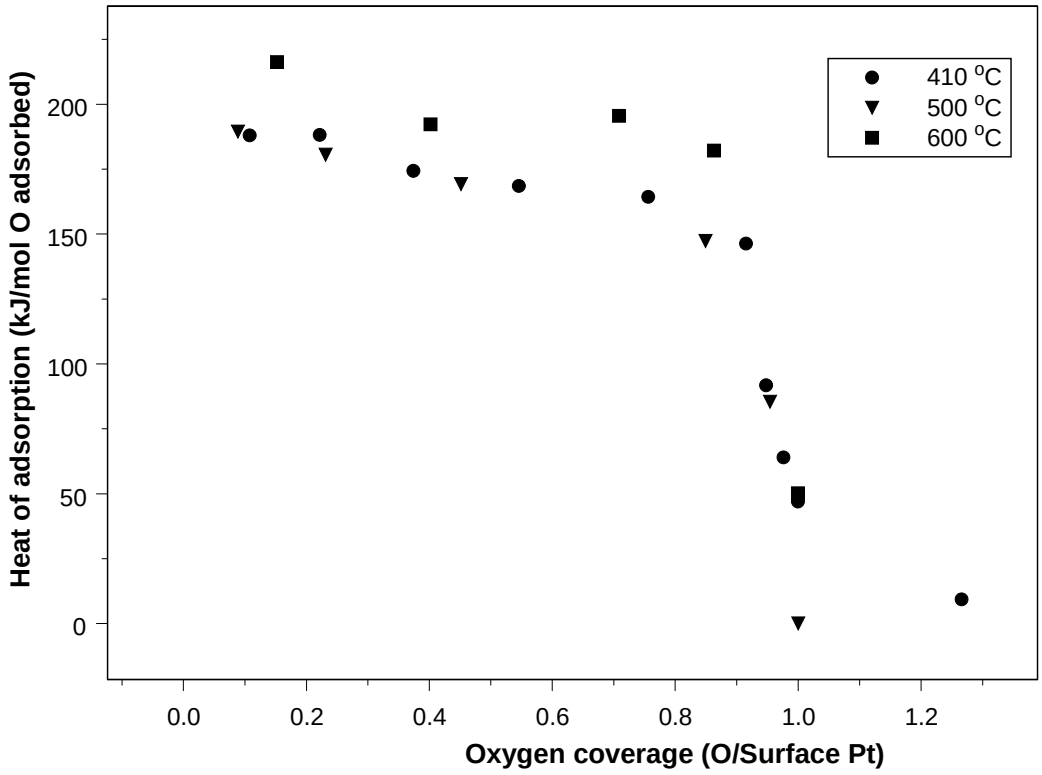

Figure 4.3: Differential heat of oxygen adsorption over 2% Pt/γ-Al_2O_3. The temperatures indicate the calcination temperature of the catalysts.

CO adsorption heats shown in Figure 4.4 were also plotted against the fractional coverage; the coverage values were normalized to the saturation values as measured by calorimetry. Carbon monoxide adsorption heats do not exhibit any structure sensitivity; the heat of adsorption data for all catalysts fell on the same curve. The initial heats of adsorption and adsorption heats at saturation agree well with the literature data (Table 2.3) as well as the isosteric heats of adsorption measured by Dulaurent and Bianchi (2000).

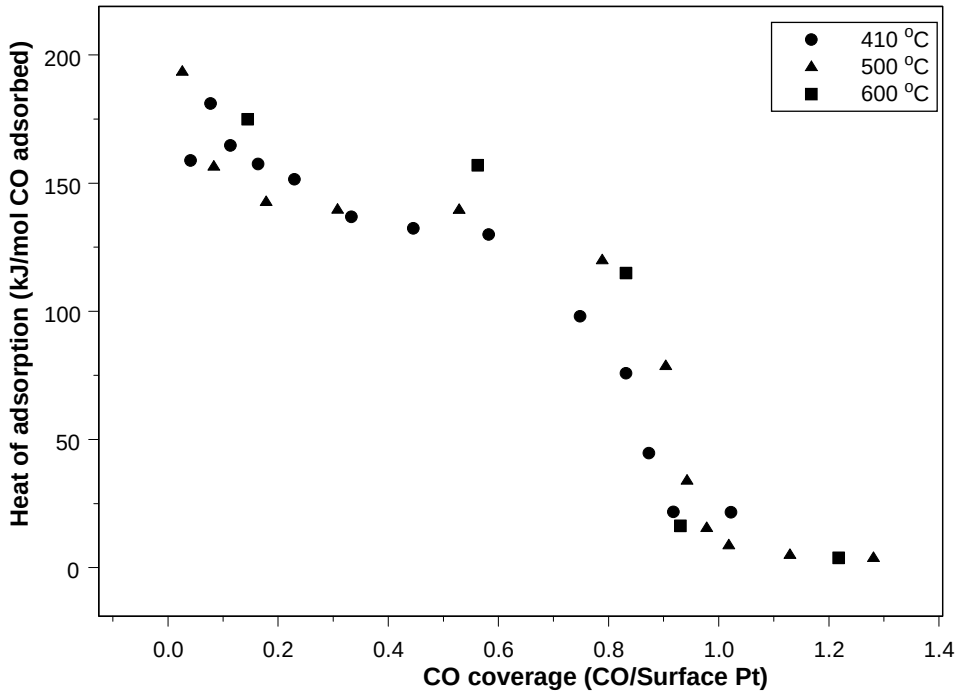

Figure 4.4: Differential heat of carbon monoxide adsorption over 2% Pt//γ-Al_2O_3. The temperatures indicate the calcination temperature of the catalysts.

The number of moles of gas adsorbed at saturation per gram catalyst is plotted against the calcination temperature in Figure 4.5. The decrease in the adsorbed gas amounts is consistent with the decrease in metal dispersions (Table 4.1). The data in Figure 4.5 has some general characteristic trends. First of all, adsorbed oxygen amounts are consistently lower than that of carbon monoxide and hydrogen. Second, the decrease in adsorbed oxygen amounts with dispersion is not as pronounced as observed in hydrogen or carbon monoxide.

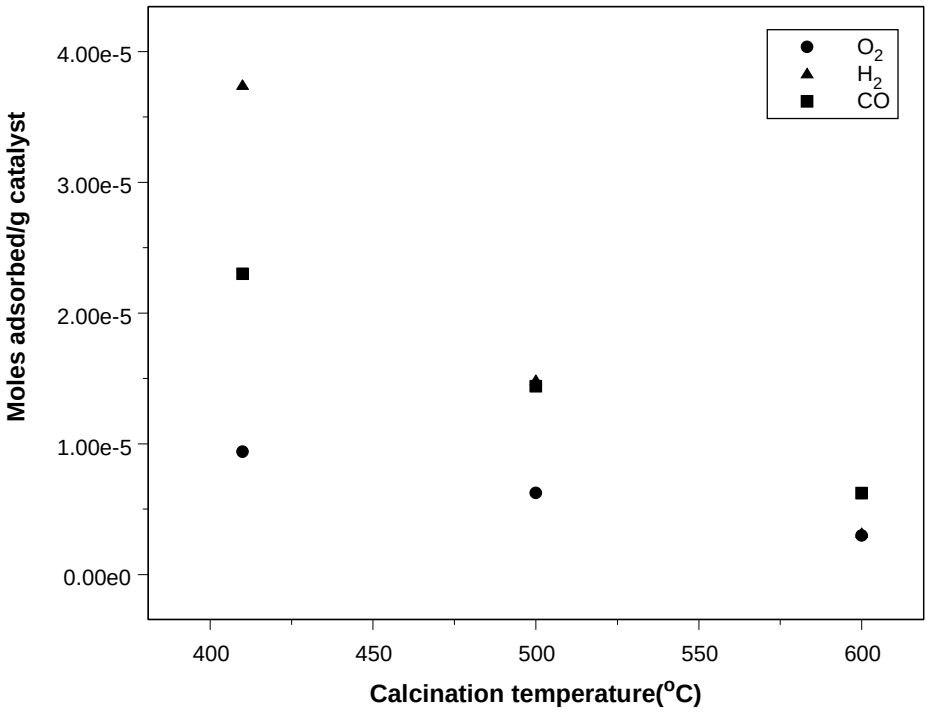

Figure 4.5: The amount of gas adsorbed at saturation as a function of catalyst calcination temperature.

Finally, on the catalyst calcined at 600 ^{o}C, the amount of hydrogen, oxygen and CO adsorbed approaches to similar values. Adsorbed hydrogen amounts are about twice as much as adsorbed CO or even larger for adsorbed oxygen amounts. This is believed to be due to a weakly bound hydrogen that exists on the metal surfaces at H:M stoichiometries greater than 1 (Savargaonkar et al., 1998).

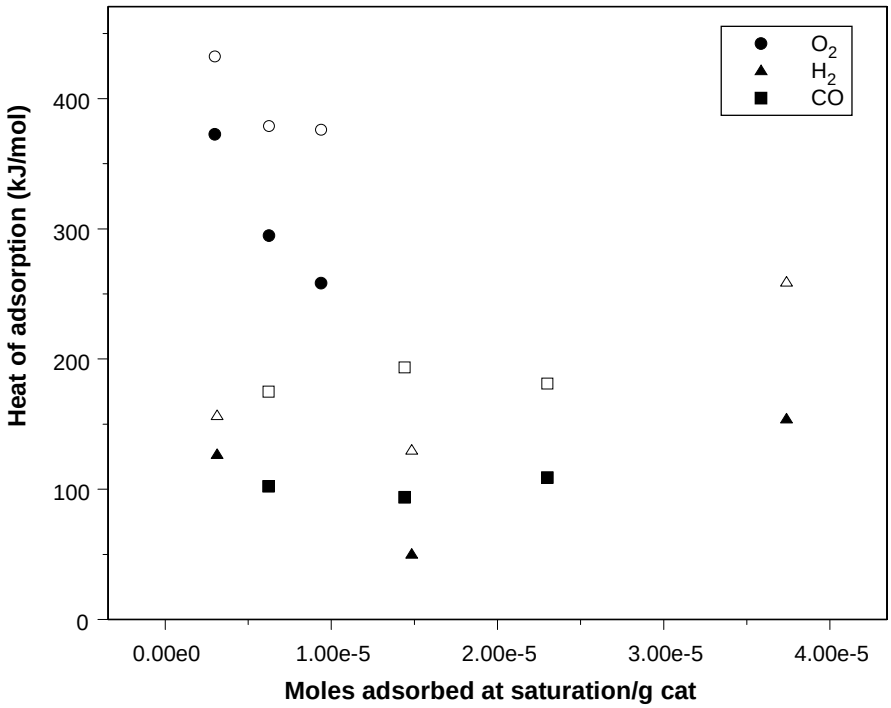

Figure 4.6: Initial (open symbols) and integral (dark symbols) heats of adsorption of hydrogen, oxygen and carbon monoxide as a function of amount of gas adsorbed at saturation.

In order to compare adsorption energetics, initial (open symbols) and integral (dark symbols) adsorption heats of oxygen, hydrogen and carbon monoxide were plotted in Figure 4.6 as a function of the amount of gas adsorbed at saturation. From Figure 4.6, one can deduce that neither initial nor integral heats of adsorption do not show a trend with changing metal particle size. It is important to note here that the oxygen adsorption heat data show a systematic decrease with decreasing particle size and the data

point pertinent to the smallest particle size distribution catalyst show an increase in both initial and integral heats.

Finally, in order to demonstrate the relative change in the adsorbent-adsorbate relationships with the metal particle size, data in Figures 4.1 - 4.3 were replotted in Figure 4.7 and 4.8. In Figure 4.7 the heats of adsorption of oxygen, carbon monoxide and hydrogen were plotted for the catalyst calcined at 410 ^{o}C, while in Figure 4.8 the heats of adsorption of oxygen, carbon monoxide and hydrogen were plotted for the catalyst calcined at 600 ^{o}C.

From Figure 4.7 one can easily deduce that hydrogen adsorption sites have a broader site energy distribution, the intermediate and low adsorption sites are not observed for carbon monoxide and oxygen. Carbon monoxide and oxygen adsorption energetics follow similar trends, which are not influenced by the metal particle size, while hydrogen adsorption site energy distribution is significantly altered by the particle size.

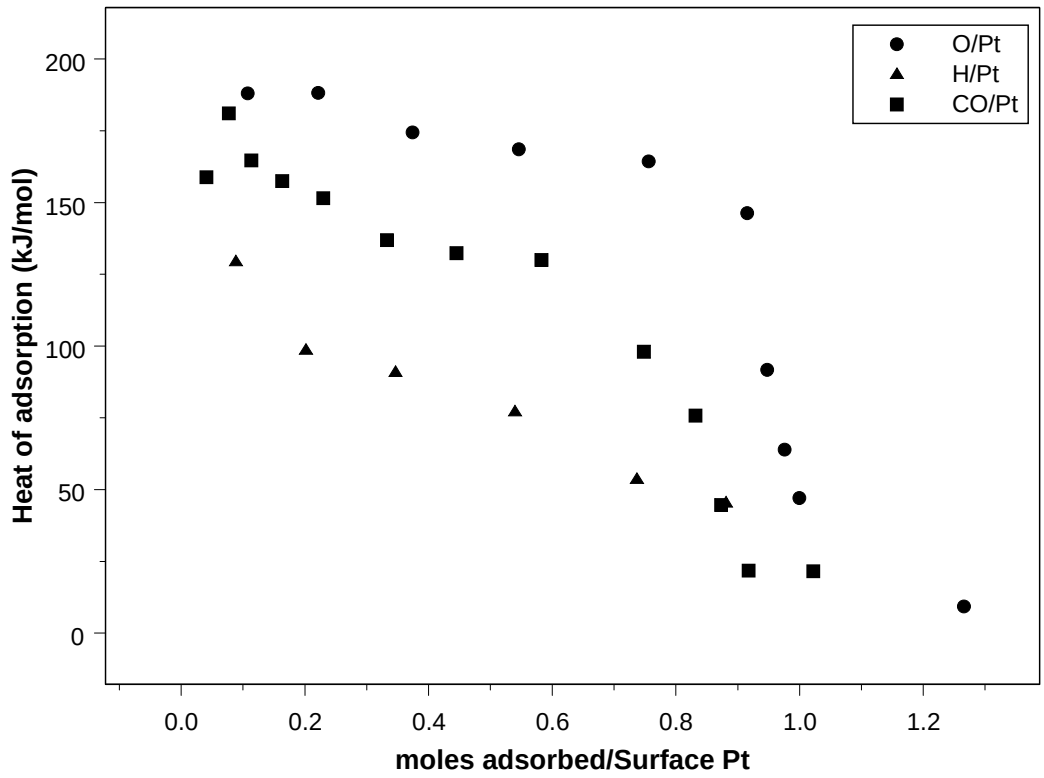

Figure 4.7: The heats of adsorption of hydrogen, oxygen and carbon monoxide over catalyst calcined at 410 ^{o}C.

On the other hand, over catalyst calcined at 600 ^{o}C CO and O heat of adsorption curves follow similar trends, energetically and for the coverages at which they saturate the surface, while hydrogen adsorption heats exhibit a drastic decrease from high initial heats of adsorption to a very low heats of adsorption, indicating that sites with intermediate heats are completely lost.

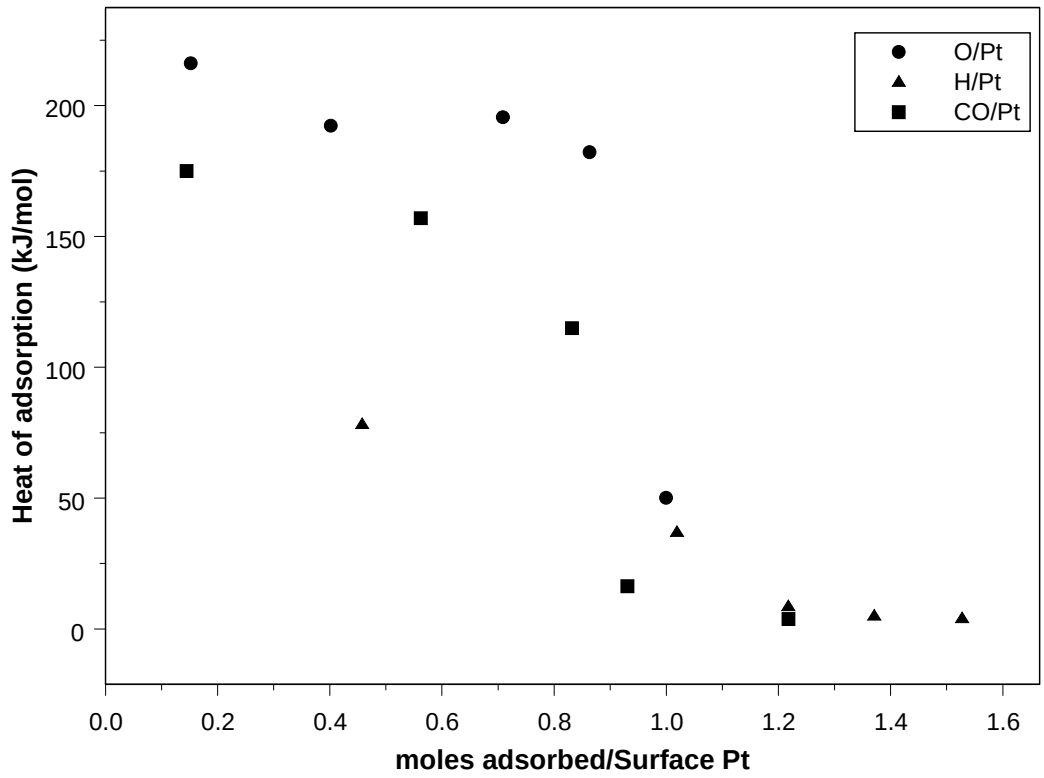

Figure 4.8: The heats of adsorption of hydrogen, oxygen and carbon monoxide over catalyst calcined at 600 ^{o}C.

CHAPTER 5

CONCLUSION

The structure sensitivity of hydrogen, oxygen and carbon monoxide was studied by adsorption calorimetry. The structure sensitivity of hydrogen chemisorption was observed consistent with the previous studies (Narayan and King, 1998; Savargoankar et al. 1998). On the other hand, the changes in the metal particle size did not reflect itself consistently to the initial and integral heats of adsorption of CO and oxygen adsorption heats. CO and oxygen adsorption isotherms and heat of adsorption data resembled each other closely indicating that these molecules compete for the same kind of sites. The site energy distributions measured by adsorption calorimetry indicated that as the particle size decreased the site density of intermediate heats decreased.

REFERENCES

Akemann, W., Friedrich, K.A., Linke, U., Stimming, U., (1998), "The catalytic oxidation of carbon monoxide at the platinum/electrolyte interface investigated by optical second harmonic generation (SHG): comparison of Pt(111) and Pt(997) electrode surfaces", Surface Science , Vol. 402-404, pp. 571-575

Auroux, A., (1994), "Thermal Methods: Calorimetry, Differential Thermal Analysis and Thermogravimetry", pp 611-650 in "Catalyst Characterization: Physical Techniques for Solid Materials" Imelik, B, and J.C. Verdine, eds. Plenium Press, New York.

Brown, W. A., Kose, R., King, D. A., (1998), "Femtomole Adsorption Calorimetry on Single-Crystal Surfaces", Chemical Reviews, Vol. 98, pp. 797-831

Campbell, C.T., Ertl, G., Kuipers, H., Segner, J., (1981), "A molecular beam study of the adsorption and desorption of oxygen from a Pt(111) surface", Surface Science, Vol. 107, Iss. 1, pp. 220-236

Cortright, R. D., Dumesic, J. A., (1995), "Effects of Potassium on Silica - Supported Pt and Pt/Sn Catalysts for Isobutane Dehydrogenation", Journal of Catalysis, Vol. 157, pp. 576-583

Cudok, A., Froitzheim, H., Hess, G., (1994), "Kinetics of the dissociative adsorption of O_2 on Pt(111): a TREELS study", Surface Science, Vol. 307-309, Iss. 2,pp. 761-767

Doraiswamy, L. K., (1991), "Catalytic reactions and reactors: A surface science approach", Progress in Surface Science, Vol. 37, pp. 1-277

Dulaurent, O., Bianchi, D., (2000), "Adsorption isobars for CO on a Pt/Al_2O_3 catalyst at high temperatures using FTIR spectroscopy: isosteric heat of adsorption and adsorption model", Applied Catalysis A: General, Vol. 196, pp. 271-280

Gland, J. L., Sexton, B. A., Fisher, G. B., (1980), "Oxygen interactions with the Pt(111) surface", Surface Science., Vol. 95, pp. 587-602

Gracia, F.J. , Bollmann, L., Wolf, E.E., Miller, J.T., Kropf, A.J., (2003), "In situ FTIR, EXAFS, and activity studies of the effect of crystallite size on silica-supported Pt oxidation catalysts", Journal of Catalysis, Vol. 220, Iss. 2, pp. 382-391

Hammer, B., Nielsen, O. H., Norskov, J. K., (1997), "Structure sensitivity in adsorption: CO interaction with stepped and reconstructed Pt surfaces", Catalysis Letters, Vol. 46, pp. 31-35

Karmazyn, A. D., Fiorin, V., Jenkins, S. J., King, D. A., (2003) "First-principles theory and microcalorimetry of CO adsorption on the {2 1 1} surfaces of Pt and Ni", Surface Science, Vol. 538, Iss. 3,pp. 171-183

Kumar, N., King, T. S., Vigil, R. D., (2000), "A portal model for structure sensitive hydrogen adsorption on Ru–Ag/SiO_2 catalysts", Chemical Engineering Science, Vol. 55, Iss. 21, pp. 4973-4979

McEwen, J. S., Payne, S. H., Kreuzer, H. J., Kinne, M., Denecke, R., Steinrück, H. P., (2003), "Adsorption and desorption of CO on Pt(1 1 1): a comprehensive analysis", Surface Science, Vol. 545, Iss. 1-2,pp. 47-69

Monroe , D. R., Merrill, R. P., (1980), "Adsorption of Oxygen on Pt(111) and Its Reactivity to Hydrogen and Carbon Monoxide", Journal of Catalysis, Vol. 65, pp. 461-469

Narayan, R. L., King, T. S., (1998) "Hydrogen adsorption states on silica-supported Ru–Ag and Ru–Cu bimetallic catalysts investigated via microcalorimetry", Thermochimica Acta, Vol. 312, Iss. 1-2,pp. 105-114

Nolan, P. D., Lutz, B. R., Tanaka, P. L., Davis, J. E., Mullins, C. B., (1999), "Molecularly chemisorbed intermediates to oxygen adsorption on Pt(111): A molecular beam and electron energy-loss spectroscopy study", Journal of Chemical Physics, Vol. 111, pp. 3696-3704

Norskov, J. K. , Bligaard, T. , Logadottir, A., Bahn, S. , Hansen, L.B. , Bollinger, M., Bengaard, H., Hammer, B., Slivancanin, Z., Mavrikakis, M., Xu, Y., Dahl, S., Jakobsen, C. J. H., (2002), "Universality in Heterogeneous Catalysis", Journal of Catalysis, Vol. 209, Iss. 2, pp. 275-278

Puglia, C., Nilsson, A., Hernnas, B., Karis, O., Bennich, P., Martensson, N., (1995), "Physisorbed, chemisorbed and dissociated O2 on Pt(111) studied by different core level spectroscopy methods", Surface Science, Vol. 342, Iss.1-3, pp. 119-133

Savargaonkar, N., Narayan, R. L., Pruski, M., Uner, D. O., King, T. S., (1998), "Structure Sensitive Hydrogen Adsorption: Effect of Ag on Ru/SiO_2Catalysts", Journal of Catalysis, Vol. 178, Iss. 1, pp. 26-33

Savargaonkar, N., Uner, D., Pruski, M., King, T. S., (2002), "Kinetics of hydrogen adsorption and desorption on silica supported Pt, Rh and Ru catalysts studied by solid state ^{1}H-NMR", Langmuir, Vol. 18, pp. 4005-4009

Schimpf, S., Lucas, M., Mohra, C., Rodemerck, U., Brückner, A., Radnik, J., Hofmeister, H., Claus, P., (2002), "Supported gold nanoparticles: in-depth catalyst characterization and application in hydrogenation and oxidation reactions", Catalysis Today Vol. 72, pp. 63–78

Schwaha, K., Bechtold, E., (1977), "The adsorption of oxygen on the stepped Pt(S)-[9(111) × (111)] face", Surface Science, Vol. 65, Iss. 1, pp. 277-286

Sharma, S. B., Miller, J. T., Dumesic, J. A., (1994) "Microcalorimetric Study of Silica- and Zeolite-Supported Platinum Catalysts", Journal of Catalysis, Vol. 148, pp. 198-204

Sljivancanin, Z., Hammer, B., (2002), "Oxygen dissociation at close-packed Pt terraces, Pt steps, and Ag-covered Pt steps studied with density functional theory", Surface Science, Vol. 515, Iss. 1,pp. 235-244

Solinas, V., Ferino, I., (1998), "Microcalorimetric characterisation of acid-basic catalysts", Catalysis Today, Vol. 41, pp. 179-189

Strohl, J, King, T. S., Personal Communication.

Thomas, j. M., Thomas, W. J., (1997), "Principles and Practice of Heterogenous Catalysis", 2nd Edition, VCH Publishing Inc., Weinheim

Tong, Y. Y., Van der Klink, J. J., (1995), "Local metal to non-metal transition on oxygen-covered platinum particles from ^{195}Pt nuclear magnetic resonance", Journal of Physics: Condense Matter, Vol. 7, pp. 2447-2459

Uner, D., Tapan, N. A., Ozen, I., Uner, M., (2003), "Oxygen adsorption on Pt/TiO_2 catalysts", Applied Catalysis A: General, Vol. 251, Iss. 2, pp. 225-234

Uner, D. O., Pruski, M., King, T. S., (1995), "Optimization of the Volumetric Hydrogen Chemisorption Technique for Dispersions of Ru/SiO_2 Catalysts", Journal of Catalysis, Vol. 156, pp. 60-64

VanderWiel, D. P., Pruski, M., King, T. S., (1999), "A Kinetic Study on the Adsorption and Reaction of Hydrogen over Silica-Supported Ruthenium and Silver–Ruthenium Catalysts during the Hydrogenation of Carbon Monoxide", Journal of Catalysis, Vol. 188, pp. 186-202

Wang, H., Tobin, R.G., Lambert, D. K., Di Maggio, C.L., Fisher, G.B., (1997), "Adsorption and dissociation of oxygen on Pt(335)", Surface Science, Vol. 372, Iss. 1-3,pp. 267-278

Wartnaby, C. E., Stuck, A., Yeo, Y. Y., King, D. A., (1996), "Microcalorimetric Heats of Adsorption for CO, NO, and Oxygen on Pt{110}", Journal of Physical Chemistry, Vol. 100, pp. 12483-12488

Tapan, N. A., (1996), "Adsorption dynamics and reaction kinetics at gas-solid interfaces: applications in catalysis and gas sensors", MS. Thesis, Middle East Technical University, Ankara, Turkey.

Yeo, Y. Y., Vattunoe, L., King, D. A., (1997), "Calorimetric heats for CO and oxygen adsorption and for the catalytic CO reaction on Pt{111}", Journal of Chemical Physics, Vol. 106, pp. 392-403

Zafiris, G. S., Gorte, R. J., (1993), "CO Oxidation on Pt/α-Al2O3(0001): Evidence for Structure Sensitive", Journal of Catalysis, Vol. 140, pp. 418-423

APPENDIX A

ADSORPTION THERMODYNAMICS

The energy released during adsorption, minus any work done by the system, is spent as heat warming the adsorption system and is measured by microcalorimeter. The term "differential heat" refers to the change in internal energy. Between the adsorbed and gaseous states following a path which no work is done, i.e.,

$$q_d = U_g - U_a \tag{A.1}$$

where U_g is the molar internal energy of the gas and U_a is the molar internal energy of the adsorbate. The sign convention for q_d is such that an exothermic process, such as adsorption, has a positive heat.

In the usual calorimetric experiment the adsorption surface area is constant and the substrate is assumed to be thermodynamically inert, so that the only work done is the gas-phase pressure-volume work, the heat of compression, q_c which may be shown as:

$$q_c = -P\frac{dV_g}{dn_a} \approx RT \qquad \text{(A.2)}$$

Here, P and V_g are the gas-phase pressure and volume and n_a is the number of moles of adsorbate. Since q_c is the order of RT, the calorimetric heat, q_{cal}, measured in an experiment for a fully reversible process is:

$$q_{cal} = q_d + RT \qquad \text{(A.3)}$$

Assuming that the solid substrate is inert, then at equilibrium the chemical potential, μ, of the adsorbate and the gas phase should change identically for any perturbation of the system. The adsorbed gas-phase chemical potential can be given with respect to temperature , T, pressure, P, adsorbate area, α, and the number of adsorbatemolecules, n_a, as

$$d\mu_a = -S_a dT + V_a dp + \left(\frac{\partial\mu}{\partial\alpha}\right)_{T,P,n_a} d\alpha + \left(\frac{\partial\mu}{\partial n_a}\right)_{T,P,\alpha} dn_a \qquad \text{(A.4)}$$

where S_a is the differential entropy and V_a is the differential volume with respect to n_a at fixed temperature, pressure, and adsorbate surface area (α). If we apply isosteric constraint that the adsorbate surface area and the number of adsorbate atoms are constant, the last terms vanish. For the gas phase:

$$d\mu_g = -S_g dT + V_g dP \qquad \text{(A.5)}$$

At equilibrium, $d\mu_a = d\mu_g$ and, hence:

$$\Delta V_{g-a}\left(\frac{\partial P}{\partial T}\right)_{\alpha,n_a} = \Delta S_{g-a} \qquad \text{(A.6)}$$

where ΔS_{g-a} and ΔV_{g-a} are the entropy and volume change that occur upon adsorption. If we assume that the gas is ideal and neglect the volume of the adsorbate, then the Clausius-Clapeyron relationship is obtained:

$$-R\left(\frac{\partial \ln P}{\partial\left(1/T\right)}\right)_{\alpha,n_a} = T\Delta S_{g-a} \qquad \text{(A.7)}$$

The term on the right-hand side is equal to the heat released in a reversible phase change, and this corresponds to a path for which the only work done is gas expansion at constant temperature and pressure. Hence $T\Delta S_{g-a} = q_d + RT$. The term on the left-hand side is the isosteric heat, q_{st}, measured in an experiment at equilibrium.

APPENDIX B

SAMPLE DISPERSION CALCULATION

To determine the dispersion, percentage of metal exposed to gas contact, hydrogen chemisorption experiments were performed for all the catalysts. The experimental procedure for the hydrogen chemisorption experiment is given below:

P_1 is the gas pressure measured when the gas is in the V_1 (Valve 1, valve 2 and valve 3 are closed).

P_2 is the gas pressure measured when the gas is in the V_2, at equlibrium with the catalyst (Valve 1 and valve 2 are closed, valve 3 is opened).

P_3 is the gas pressure measured after valve 2 is closed, equal to pressure of the gas remaining in the sample chamber (Valve 1, valve 2 and valve 3 are closed).

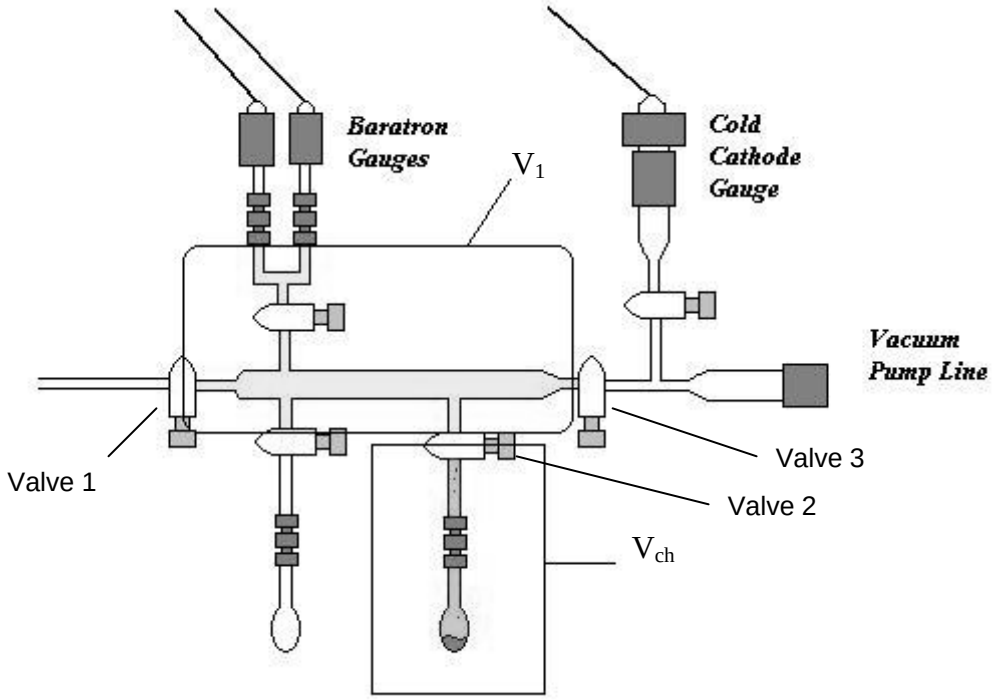

Figure B.1: Home built multi-port high-vacuum Pyrex glass manifold.

- Weight 1 gr of catalyst and place it in the Pyrex sample cell.
- Connect the cell to the sample port of the manifold by Swagelok UltraTorr Union and place heating mantle around the sample cell.
- Start heating the sample.
- Dose approximately 100 Torr of helium into the manifold, at 423 K for about 30 min to remove the residual water on the sample.
- Evacuate the sample, then dose 100 Torr of H_2 on the sample and raise the temperature gradually to 623 K.
- At this temperature evacuate the sample, dose fresh hydrogen at 750 Torr for 30 min.
- Replenish the hydrogen every 30 min. until the catalyst is exposed to hydrogen atmosphere at 623 K for at least 2 hours.

- After the reduction process, evacute the system for 1 hour and then cooled down the catalyst to room temperature during final evacuation.
- For dead-volume measurements, dose He to the system at a pessure between 0-50 Torrs and record the pressure data (P_1 and P_2).
- Dose hydrogen at a pressure of 5 Torr to the system and wait for the equilibrium (no change in the gas pressure for 10 min.). Record P_1, P_2 and P_3.
- Repeat dosing hydrogen at pressures of 10, 20 and 40 Torrs to the system and wait for the equilibrium (no change in the gas pressure for 10 min.). Record P_1, P_2 and P_3.
- After collecting data for total hydrogen adsorption evacute the system for 10 min at room temperature. This procedure, by convention, removes the weakly bound hydrogen, leaving only strongly bound hydrogen over the surface. A second isotherm obtained afterwards give the weakly bound hydrogen amounts as described below.
- Repeat dosing hydrogen at pressures of 5, 10, 20 and 40 Torrs to the system and wait for the equilibrium (no change in the gas pressure for 10 min.). Record P_1, P_2 and P_3.

The data obtained in these experiments are given in tables B.1, C.2 and C.3. The experimental data consists of the changing pressure values with the expansion and the adsorption of the gas in the constant total volume manifold. The calculation performed to obtain the dispersion value is as follows:

Table B.1 Pressure data obtained for hydrogen adsorption experiment of 2%Pt/Al_2O_3 calcined at 410 °C.

Adsorption Mode	P_1 (Torrs)	P_2 (Torrs)	P_3 (Torrs)
Total	5.02	0.215	0.217
	10.7	8.74	8.78
	30.2	26.7	26.8
	55.9	51.1	51.2
Weak	5.29	3.46	3.48
	13.3	11.6	11.6
	30.4	27.3	27.4
	53.6	49.3	49.4

$V_1 = 162\text{cm}^3$

$T = 299.15\text{K}$

Pressure data obtained in volume measurement with He;

$P_1 = 53.1\text{Torrs}$

$P_2 = 44.6\text{Torrs}$

$P_3 = 44.7\text{Torrs}$

By assuming gasses at these pressures obeys the Ideal gas law and the data for the expansion of He on the sytem one can calculate the volume occupied by the gas in the system as follows;

$P_1 * V_1 = P_2 * V_2$

$53.1\text{Torrs} * 162\text{cm}^3 = 44.6\text{Torrs} * V_2$

$V_2 = 192.87\text{cm}^3$

$V_{ch} = V_2 - V_1 = 192.87\text{cm}^3 - 162\text{cm}^3 = 30.87\text{cm}^3$

The amount of gas present at known volumes for dose one can be calculated as;

$$R = 82.056 \frac{\text{cm}^3 * \text{atm}}{\text{mol} * \text{K}}$$

$$N_{1,1} = \frac{P_{1,1} * V_1}{R * T} = \frac{\left(\frac{5.02}{760}\text{atm}\right) * 162\text{cm}^3}{82.056 \frac{\text{cm}^3 * \text{atm}}{\text{mol} * \text{K}} * 299.15\text{K}} = 4.359 * 10^{-5}\text{mol}$$

$$N_{2,1} = \frac{P_{2,1} * V_2}{R * T} = \frac{\left(\frac{0.215}{760}\text{atm}\right) * 192.87\text{cm}^3}{82.056\frac{\text{cm}^3 * \text{atm}}{\text{mol} * \text{K}} * 299.15\text{K}} = 2.223 * 10^{-6}\,\text{mol}$$

$$N_{ch,1} = \frac{P_{3,1} * V_{ch}}{R * T} = \frac{\left(\frac{0.217}{760}\text{atm}\right) * 30.87\text{cm}^3}{82.056\frac{\text{cm}^3 * \text{atm}}{\text{mol} * \text{K}} * 299.15\text{K}} = 3.591 * 10^{-7}\,\text{mol}$$

The adsorption at dose one;

$$N_{ads,1} = N_{1,1} - N_{2,1} = 4.359 * 10^{-5} - 2.223 * 10^{-6} = 4.137 * 10^{-5}\,\text{mol.}$$

For dose two, amount of gas present at known volumes are;

$$N_{1,2} = \frac{P_{1,2} * V_1}{R * T} = \frac{\left(\frac{10.7}{760}\text{atm}\right) * 162\text{cm}^3}{82.056\frac{\text{cm}^3 * \text{atm}}{\text{mol} * \text{K}} * 299.15\text{K}} = 9.292 * 10^{-5}\,\text{mol}$$

$$N_{2,2} = \frac{P_{2,2} * V_2}{R * T} = \frac{\left(\frac{8.74}{760}\text{atm}\right) * 192.87\text{cm}^3}{82.056\frac{\text{cm}^3 * \text{atm}}{\text{mol} * \text{K}} * 299.15\text{K}} = 9.036 * 10^{-5}\,\text{mol}$$

$$N_{ch,2} = \frac{P_{3,2} * V_{ch}}{R * T} = \frac{\left(\frac{8.78}{760}\text{atm}\right) * 30.87\text{cm}^3}{82.056\frac{\text{cm}^3 * \text{atm}}{\text{mol} * \text{K}} * 299.15\text{K}} = 1.453 * 10^{-5}\,\text{mol}$$

The adsorption at dose two;

$$N_{ads,2} = N_{1,2} - N_{2,2} + N_{ch,1} = 9.292*10^{-5} - 9.036*10^{-5} + 3.591*10^{-7} = 2.915*10^{-6}\,\text{mol.}$$

For dose three, amount of gas present at known volumes are;

$$N_{1,3} = \frac{P_{1,3}*V_1}{R*T} = \frac{\left(\frac{30.2}{760}\text{atm}\right)*162\text{cm}^3}{82.056\frac{\text{cm}^3*\text{atm}}{\text{mol}*\text{K}}*299.15\text{K}} = 2.622*10^{-4}\,\text{mol}$$

$$N_{2,3} = \frac{P_{2,3}*V_2}{R*T} = \frac{\left(\frac{26.7}{760}\text{atm}\right)*192.87\text{cm}^3}{82.056\frac{\text{cm}^3*\text{atm}}{\text{mol}*\text{K}}*299.15\text{K}} = 2.760*10^{-4}\,\text{mol}$$

$$N_{ch,3} = \frac{P_{3,3}*V_{ch}}{R*T} = \frac{\left(\frac{26.8}{760}\text{atm}\right)*30.87\text{cm}^3}{82.056\frac{\text{cm}^3*\text{atm}}{\text{mol}*\text{K}}*299.15\text{K}} = 4.435*10^{-5}\,\text{mol}$$

The adsorption at dose three;

$$N_{ads,3} = N_{1,3} - N_{2,3} + N_{ch,2} = 2.622*10^{-4} - 2.760*10^{-4} + 1.453*10^{-5} = 7.359*10^{-7}\,\text{mol.}$$

For dose four, amount of gas present at known volumes are;

$$N_{1,4} = \frac{P_{1,4} * V_1}{R * T} = \frac{\left(\frac{55.9}{760}\text{atm}\right) * 162\text{cm}^3}{82.056\frac{\text{cm}^3 * \text{atm}}{\text{mol} * \text{K}} * 299.15\text{K}} = 4.854 * 10^{-4}\,\text{mol}$$

$$N_{2,4} = \frac{P_{2,4} * V_2}{R * T} = \frac{\left(\frac{51.1}{760}\text{atm}\right) * 192.87\text{cm}^3}{82.056\frac{\text{cm}^3 * \text{atm}}{\text{mol} * \text{K}} * 299.15\text{K}} = 5.283 * 10^{-4}\,\text{mol}$$

$$N_{ch,4} = \frac{P_{3,4} * V_{ch}}{R * T} = \frac{\left(\frac{51.2}{760}\text{atm}\right) * 30.87\text{cm}^3}{82.056\frac{\text{cm}^3 * \text{atm}}{\text{mol} * \text{K}} * 299.15\text{K}} = 8.473 * 10^{-5}\,\text{mol}$$

The adsorption at dose four;

$$N_{ads,4} = N_{1,4} - N_{2,4} + N_{ch,3} = 4.854 * 10^{-4} - 5.283 * 10^{-4} + 4.435 * 10^{-5} = 1.466 * 10^{-6}\,\text{mol.}$$

Repeating the same calculations for the weak adsorption;

$$N_{1,1}{}^{1} = \frac{P_{1,1}{}^{1} * V_1}{R * T} = \frac{\left(\frac{5.29}{760}\text{atm}\right) * 162\text{cm}^3}{82.056\frac{\text{cm}^3 * \text{atm}}{\text{mol} * \text{K}} * 299.15\text{K}} = 4.594 * 10^{-5}\,\text{mol}$$

$$N_{2,1}{}^{1} = \frac{P_{2,1}{}^{1} * V_2}{R * T} = \frac{\left(\frac{3.46}{760}\text{atm}\right) * 192.87\text{cm}^3}{82.056\frac{\text{cm}^3 * \text{atm}}{\text{mol} * \text{K}} * 299.15\text{K}} = 3.577 * 10^{-5}\,\text{mol}$$

$$N_{ch,1}^{\ 1} = \frac{P_{3,1}^{\ 1} * V_{ch}}{R * T} = \frac{\left(\frac{3.48}{760}\text{atm}\right) * 30.87\text{cm}^3}{82.056\frac{\text{cm}^3 * \text{atm}}{\text{mol} * \text{K}} * 299.15\text{K}} = 5.759 * 10^{-6}\,\text{mol}$$

The adsorption at dose one;

$$N_{ads,1}^{\ 1} = N_{1,1}^{\ 1} - N_{2,1}^{\ 1} = 4.594 * 10^{-5} - 3.577 * 10^{-5} = 1.016 * 10^{-5}\,\text{mol.}$$

For dose two, amount of gas present at known volumes are;

$$N_{1,2}^{\ 1} = \frac{P_{1,2}^{\ 1} * V_1}{R * T} = \frac{\left(\frac{13.3}{760}\text{atm}\right) * 162\text{cm}^3}{82.056\frac{\text{cm}^3 * \text{atm}}{\text{mol} * \text{K}} * 299.15\text{K}} = 1.155 * 10^{-4}\,\text{mol}$$

$$N_{2,2}^{\ 1} = \frac{P_{2,2}^{\ 1} * V_2}{R * T} = \frac{\left(\frac{11.6}{760}\text{atm}\right) * 192.87\text{cm}^3}{82.056\frac{\text{cm}^3 * \text{atm}}{\text{mol} * \text{K}} * 299.15\text{K}} = 1.199 * 10^{-4}\,\text{mol}$$

$$N_{ch,2}^{\ 1} = \frac{P_{3,2}^{\ 1} * V_{ch}}{R * T} = \frac{\left(\frac{11.6}{760}\text{atm}\right) * 30.87\text{cm}^3}{82.056\frac{\text{cm}^3 * \text{atm}}{\text{mol} * \text{K}} * 299.15\text{K}} = 1.919 * 10^{-5}\,\text{mol}$$

The adsorption at dose two;

$$N_{ads,2}^{\ 1} = N_{1,2}^{\ 1} - N_{2,2}^{\ 1} + N_{ch,1}^{\ 1} = 1.155 * 10^{-4} - 1.199 * 10^{-4} + 5.759 * 10^{-6} = 1.324 * 10^{-6}\,\text{mol.}$$

For dose three, amount of gas present at known volumes are;

$$N_{1,3}{}^{1} = \frac{P_{1,3}{}^{1} * V_1}{R * T} = \frac{\left(\frac{30.4}{760}\text{atm}\right) * 162\text{cm}^3}{82.056\frac{\text{cm}^3 * \text{atm}}{\text{mol} * \text{K}} * 299.15\text{K}} = 2.639 * 10^{-4}\,\text{mol}$$

$$N_{2,3}{}^{1} = \frac{P_{2,3}{}^{1} * V_2}{R * T} = \frac{\left(\frac{27.3}{760}\text{atm}\right) * 192.87\text{cm}^3}{82.056\frac{\text{cm}^3 * \text{atm}}{\text{mol} * \text{K}} * 299.15\text{K}} = 2.822 * 10^{-4}\,\text{mol}$$

$$N_{ch,3}{}^{1} = \frac{P_{3,3}{}^{1} * V_{ch}}{R * T} = \frac{\left(\frac{27.4}{760}\text{atm}\right) * 30.87\text{cm}^3}{82.056\frac{\text{cm}^3 * \text{atm}}{\text{mol} * \text{K}} * 299.15\text{K}} = 4.535 * 10^{-5}\,\text{mol}$$

The adsorption at dose three;

$$N_{ads,3}{}^{1} = N_{1,3}{}^{1} - N_{2,3}{}^{1} + N_{ch,2}{}^{1} = 2.639 * 10^{-4} - 2.822 * 10^{-4} + 1.919 * 10^{-5} = 9.365 * 10^{-7}\,\text{mol.}$$

For dose four, amount of gas present at known volumes are;

$$N_{1,4}{}^{1} = \frac{P_{1,4}{}^{1} * V_1}{R * T} = \frac{\left(\frac{53.6}{760}\text{atm}\right) * 162\text{cm}^3}{82.056\frac{\text{cm}^3 * \text{atm}}{\text{mol} * \text{K}} * 299.15\text{K}} = 4.654 * 10^{-4}\,\text{mol}$$

$$N_{2,4}^{\ 1} = \frac{P_{2,4}^{\ 1} * V_2}{R * T} = \frac{\left(\frac{49.3}{760}\text{atm}\right) * 192.87\text{cm}^3}{82.056\frac{\text{cm}^3 * \text{atm}}{\text{mol} * \text{K}} * 299.15\text{K}} = 5.097 * 10^{-4}\,\text{mol}$$

$$N_{ch,4}^{\ 1} = \frac{P_{3,4}^{\ 1} * V_{ch}}{R * T} = \frac{\left(\frac{49.4}{760}\text{atm}\right) * 30.87\text{cm}^3}{82.056\frac{\text{cm}^3 * \text{atm}}{\text{mol} * \text{K}} * 299.15\text{K}} = 8.175 * 10^{-5}\,\text{mol}$$

The adsorption at dose four;

$$N_{ads,4}^{\ 1} = N_{1,4}^{\ 1} - N_{2,4}^{\ 1} + N_{ch,3}^{\ 1} = 4.654 * 10^{-4} - 5.097 * 10^{-4} + 4.535 * 10^{-5} = 1.096 * 10^{-6}\,\text{mol.}$$

To express the moles in incremental maner, adding up the adsorbed moles yields;

Table B.2 Pressure data obtained and incremental adroption calculated for hydrogen adsorption experiment of 2%Pt/Al_2O_3 calcined at 410 °C.

Adsorption Mode	P_1 (Torrs)	P_2 (Torrs)	P_3 (Torrs)	Incremental N_{ads}
Total	5.02	0.215	0.217	$4{,}137*10^{-5}$
	10.7	8.74	8.78	$4{,}428*10^{-5}$
	30.2	26.7	26.8	$4{,}502*10^{-5}$
	55.9	51.1	51.2	$4{,}649*10^{-5}$
Weak	5.29	3.46	3.48	$1{,}016*10^{-5}$
	13.3	11.6	11.6	$1{,}149*10^{-5}$
	30.4	27.3	27.4	$1{,}243*10^{-5}$
	53.6	49.3	49.4	$1{,}352*10^{-5}$

After calculating the incremental adsorbed moles, the amount of hydrogen bound to a Pt can be calculated by equation;

$$\frac{H}{Pt} = \frac{2 * N_{ads,x}}{m_{cat} * \%Pt * M_{Pt}}$$

For dose one;

$$\left[\frac{H}{Pt}\right]_1 = \frac{2 * 4.137 * 10^{-5} mol}{\frac{1g * 0.02}{195.08 \frac{g}{mol}}} = 0{,}807 \text{ ,} \qquad \left[\frac{H}{Pt}\right]_1^1 = \frac{2 * 1.016 * 10^{-5} mol}{\frac{1g * 0.02}{195.08 \frac{g}{mol}}} = 0{,}198$$

For dose two;

$$\left[\frac{H}{Pt}\right]_2 = \frac{2 * 4.428 * 10^{-5} mol}{\frac{1g * 0.02}{195.08 \frac{g}{mol}}} = 0{,}864 \text{ ,} \qquad \left[\frac{H}{Pt}\right]_2^1 = \frac{2 * 1.149 * 10^{-5} mol}{\frac{1g * 0.02}{195.08 \frac{g}{mol}}} = 0{,}224$$

For dose three;

$$\left[\frac{H}{Pt}\right]_3 = \frac{2 * 4.502 * 10^{-5} mol}{\frac{1g * 0.02}{195.08 \frac{g}{mol}}} = 0{,}878 \text{ ,} \qquad \left[\frac{H}{Pt}\right]_3^1 = \frac{2 * 1.243 * 10^{-5} mol}{\frac{1g * 0.02}{195.08 \frac{g}{mol}}} = 0{,}242$$

For dose four;

$$\left[\frac{H}{Pt}\right]_4 = \frac{2 * 4.649 * 10^{-5} mol}{\frac{1g * 0.02}{195.08 \frac{g}{mol}}} = 0{,}907 \text{ ,} \qquad \left[\frac{H}{Pt}\right]_4^1 = \frac{2 * 1.352 * 10^{-5} mol}{\frac{1g * 0.02}{195.08 \frac{g}{mol}}} = 0{,}264$$

By plotting $\frac{H}{Pt}$ vs. P_2 figure B.2 is obtained and from the figure B.2, extrapolating the data to the zero pressure (clean surface), the percents of

the total and the weak adsorbed hydrogens can be obtained. The difference between these two, total and weak adsorption, yields the percentage of the strongly bound hydrogen. The percentage of the strongly bound hydrogen is taken as the dispersion value.

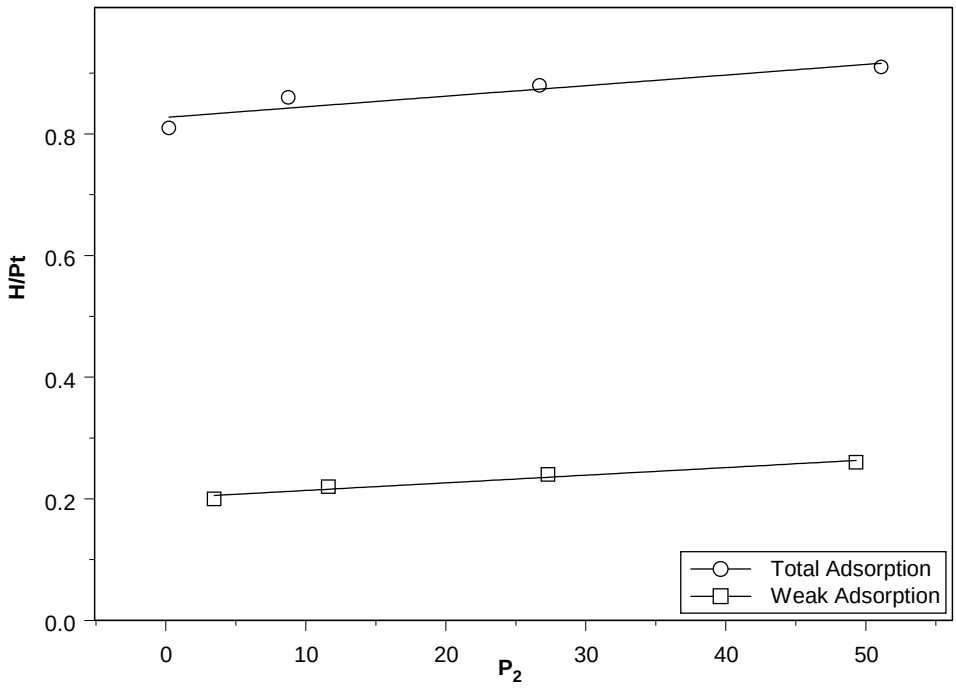

Figure B.2: Change of the Hydrogen atoms bonded to Pt atoms with H2 gas pressure on catalyst calcined at 410°C.

APPENDIX C

HYDROGEN ADSORPTION EXPERIMENT RESULTS

To determine the dispersion, percentage of metal exposed to gas contact, hydrogen adorption experiments, described in section 3.2, were performed for all the catalysts. The calculations described in Appendix B were applied to raw data. The graphical and tabulated forms of the experimental results are given below:

$T = 299.15K$

Pressure data obtained in volume measurement with He;

$P_1 = 27.7Torrs$, $P_2 = 23.2Torrs$, $P_3 = 23.3Torrs$

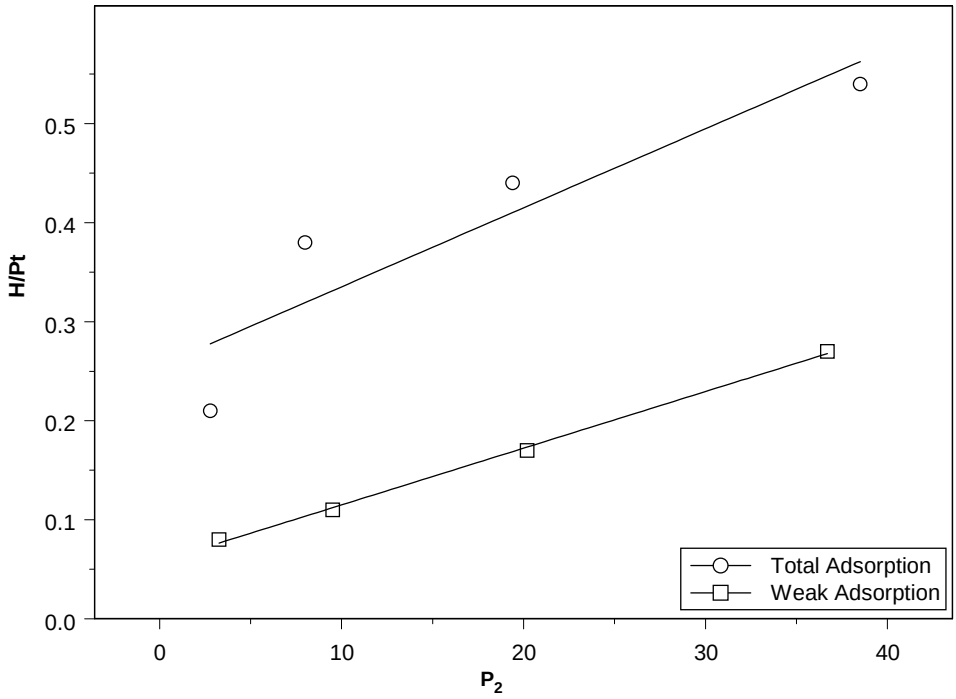

Figure C.1: Change of the Hydrogen atoms bonded to Pt atoms with H_2 gas pressure on catalyst calcined at 500°C.

Table C.1 Pressure data obtained for hydrogen adsorption experiment of 2%Pt/Al_2O_3 calcined at 500 °C.

Adsorption Mode	P_1 (Torrs)	P_2 (Torrs)	P_3 (Torrs)	H/Pt
Total	4.59	2.79	2.8	0.21
	10	8	8.78	0.38
	21.8	19.4	19.5	0.44
	42.8	38.5	38.7	0.54
Weak	4.37	3.27	3.29	0.08
	10.9	9.51	9.56	0.11
	22.6	20.2	20.3	0.17
	40.5	36.7	36.9	0.27

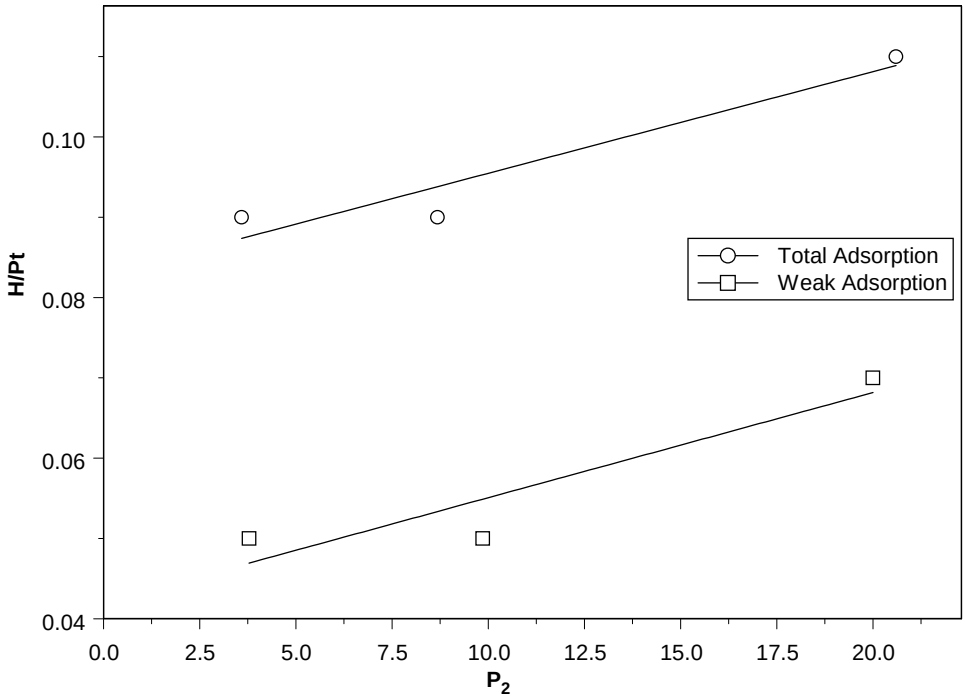

Figure C.2: Change of the Hydrogen atoms bonded to Pt atoms with H_2 gas pressure on catalyst calcined at 600°C.

$T = 299.15K$

Pressure data obtained in volume measurement with He;

$P_1 = 34.9Torrs$, $P_2 = 29.4Torrs$, $P_3 = 29.5Torrs$

Table C.2 Pressure data obtained for hydrogen adsorption experiment of 2%Pt/Al_2O_3 calcined at 600 °C.

Adsorption Mode	P_1 (Torrs)	P_2 (Torrs)	P_3 (Torrs)	H/Pt
Total	4.81	3.59	3.61	0.09
	9.63	8.68	8.72	0.09
	22.9	20.6	20.7	0.11
Weak	4.79	3.78	3.8	0.05
	11	9.86	9.88	0.05
	22	20	20.2	0.07

APPENDIX D

CUBOCTAHEDRA STRUCTURE

As mentioned in section 2, the relative amount of the corner and edge sites increases as the dispersion value increases. The diameter of the metal particle increases as the dispersion value decreases. According to the Monte Carlo simulations performed by Sthrol and King the change of the percentage to the total with dispersion is given in the Figure D.1.

Schimpf et al. has studied supported gold nanoparticles on hydrogenation and oxidation reactions. To explain the observed structure sensitivity on small nanoparticles with changing metal particle diameter, the different activites of sites and the change of the relative amounts with particle diameter were mentioned. The changing frequencies of the sites were visualized in Figure D.3.

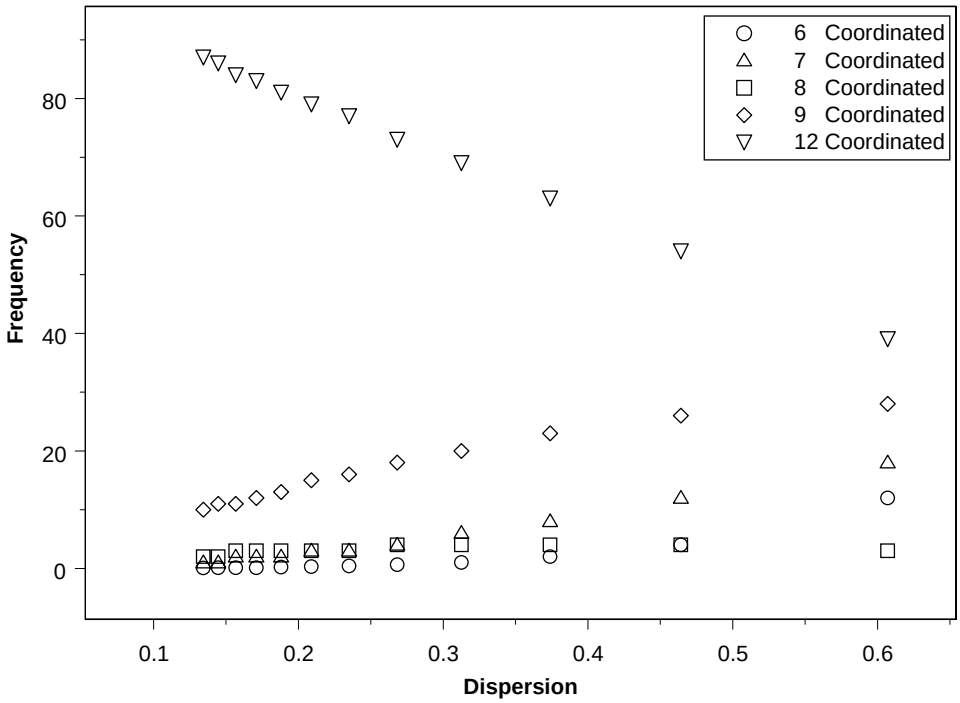

Figure D.1: Dependence of relative amounts of different coordinated atoms of Pt (Sthrol and King).

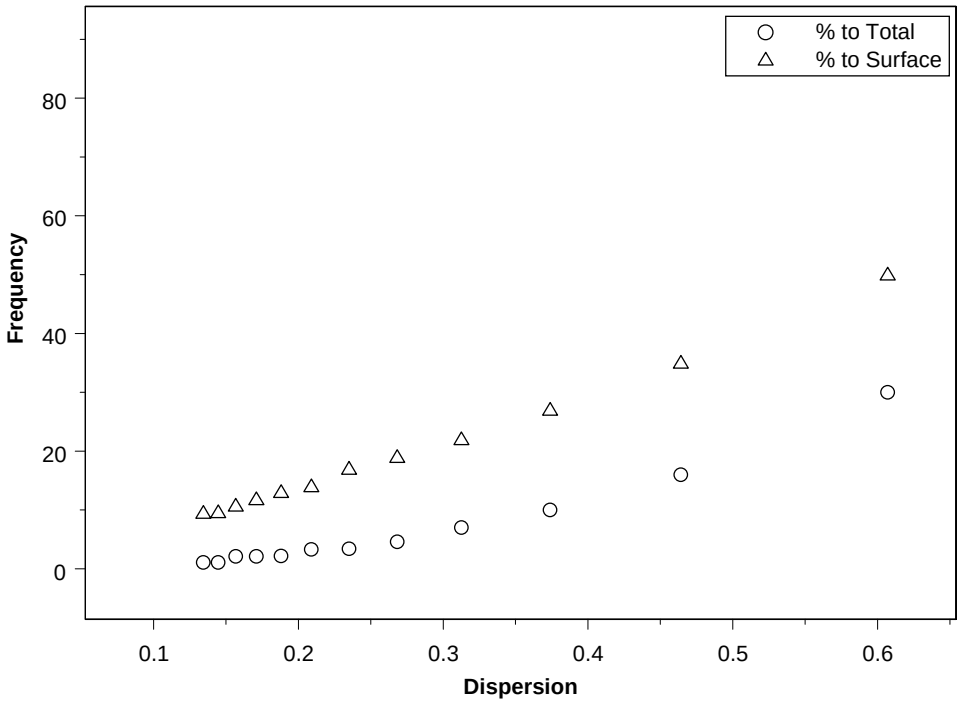

Figure D.2: Dependence of relative amounts of corner and edge sites to the total and surface of Pt. (Sthrol and King).

Table D.1 Theoretical percents of corner and edge sites present on the surface and total, according to the Monte Carlo simulations, of the 2%Pt/γ-Al_2O_3 calcined at different temperatures.

Calcination Temperature (°C)	Dispersion (%)	Frequency in the surface (%)	Frequency in the total (%)
410	0,62	52	52
500	0,20	14	9
600	0,04	4	2

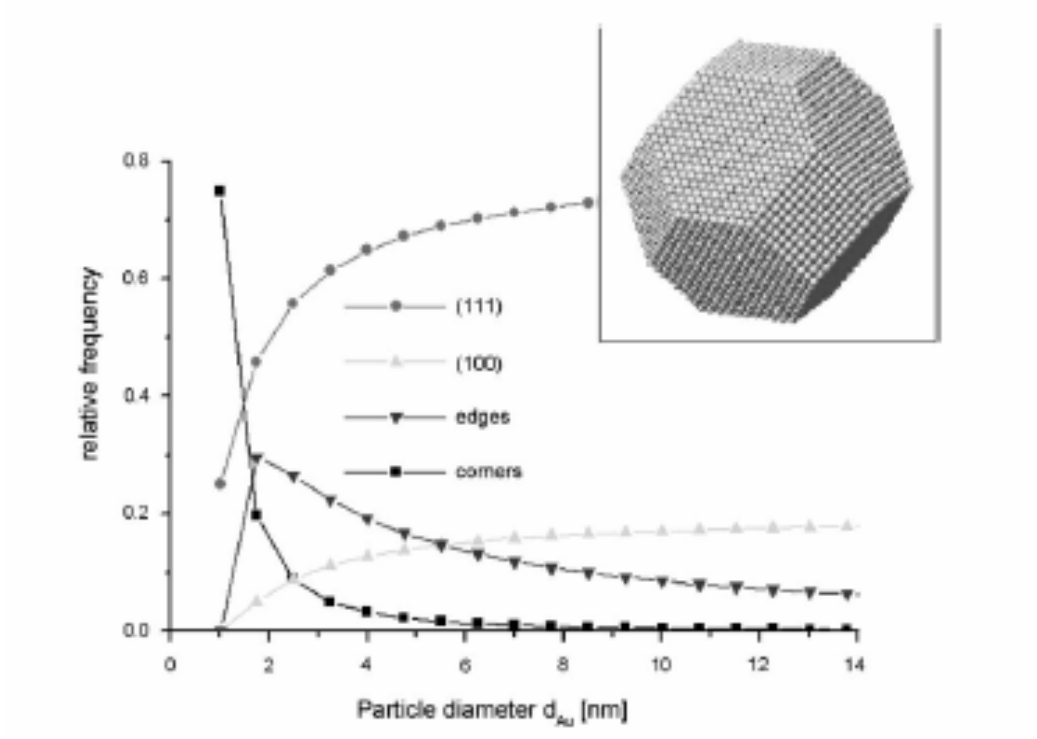

Figure D.3: Dependence of relative amounts of surface sites on particle diameter of gold particles, based on cuboctahedron model (Schimpf et al., 2002).